University of Alberta

Fabrication and properties of aluminum-carbon nanotube accumulative roll bonded composites

by

Sahar Salimi

A thesis submitted to the Faculty of Graduate Studies and Research
in partial fulfillment of the requirements for the degree of

Master of Science
in
Materials Engineering

Department of Chemical and Materials Engineering

Spring 2011
Edmonton, Alberta

Abstract

Accumulative roll bonding was adapted to fabricate a carbon nanotube reinforced aluminum matrix composite. The microstructure was investigated by transmission electron microscopy, and it was confirmed that the nanotubes were embedded into the metal matrix while maintaining their multiwalled structure. Measurements revealed that the as-received carbon nanotubes had a bimodal diameter size distribution, while only nanotubes with diameters >30 nm and more than 30 walls were retained during four consecutive rolling operations at 50% reduction.

The elastic deflection and vibration damping properties of the laminated composite were investigated by cantilever bending test and by impulse excitation method in samples with different concentrations of carbon nanotubes. Measurements by both methods revealed that a 0.23wt% concentration of nanotubes increased the elastic modulus according to the rule of mixtures and the damping behavior of the composites increased by the addition of nanotubes up to 0.1wt%.

Acknowledgment

I am greatly thankful to my supervisor, Dr. Adrian Gerlich, for his encouragement, guidance and support from the initial to the final level of my program. I am indeed deeply indebted to him. He taught me to perform research not only for the results, but also for the methods used to achieve them. It was such a great honor for me to be guided by him.

I would like to thank my committee members, Dr. Patricio Mendez and Dr. Adam Lubell for agreeing to review my work, as well as Dr. Anthony Yeung for being the chair of my examining committee.

I would like to acknowledge the Chemical and Materials engineering department and Natural Sciences and Engineering Research Council of Canada for financial support in this research. I am very grateful to my colleagues, Hossein Izadi, Matthew Dewar, Kevin Hodder, and Hannah Leibel for their help and assistance.

My parents deserve special mention for their inseparable support and prayers. It is a pleasure to thank those who made this thesis possible, George Braybrook and Martin Kupsta for assistance with the SEM and Greg Popowich and Roham Eslahpaz for TEM assistance. Finally, thanks to Katherine Jonsson and Nima Saber for useful notes whilst writing this thesis.

Table of Contents

List of Figures

List of Tables

List of abbreviations

ARB: Accumulative roll bonding

SEM: Scanning electron microscopy

EDX: Energy dispersive X-ray analysis

TEM: Transmission electron microscopy

XRD: X-ray diffraction

CNT: Carbon Nanotube

MMC: Metal matrix composite

SPD: Severe plastic deformation

1 Introduction

Accumulative roll bonding (ARB) was developed by Saito et al.[1] as a severe plastic deformation technique for refining the grain size of an alloy. In this process multiple layers of metals or alloys are stacked together and then rolled until a sufficient degree of deformation, usually around 50%, is achieved and a solid state bond between the original individual metal pieces is formed. To form the bond, sufficient pressure on the metal strips must be applied and a threshold strain value should be achieved [2]. With increasing strain and thickness reductions applied to the material, a limit is eventually reached due to work hardening applied to the metal strip [3].

A variation of the roll bonding process has been developed in which a nanoscale powder reinforcing material is dispersed between the sheets prior to rolling with the aim of producing a layer of metal matrix composite material at the interface. The process is similar to sheath-rolling involving encapsulation of macro-scale wires or particles. This has been discussed elsewhere [4].

ARB has the advantage of increasing the strength of the matrix material via grain refinement and has the potential to achieve high concentrations of Carbon nano tubes (CNT) material in the composite since the process can be repeated for several passes by changing the parameters of the process. Moreover, it has been proposed that reinforcing fibers are dispersed and are preferentially aligned in the rolling direction during roll bonding of CNT metal matrix composites [5]. One potential benefit of this process is that the rate of entanglement in the CNT base material may be reduced during fabrication using this process, particularly with increased strains during repeated rolling operations.

Some techniques such as hot extrusion, equal channel angular pressing, shockwave consolidation, and mechanical alloying [6-8] have also been used applied for producing CNT metal matrix composites, however a number of technical issues can be caused during synthesis. For example, the processing

route may result in damage of the nanotube structure, poor interfacial bonding between CNTs and metal matrix, or agglomeration of the CNTs [9].

The number of the cycles and the dispersion of the CNTs at the interface of the metal sheets have a significant effect in promoting the bond strength at the interface of the composites. At higher surface densities, the carbon nanotube clusters tend to form due to their high surface tension and the nanotubes may become tangled in these bundles, which offer poor load transfer to the surrounding matrix [10].

Although possible damage to the CNTs has been suggested during roll bonding of Al-CNT composite [5], the factors controlling the CNT stability during the process have never been examined. This is a particular concern, since potential to distribute the CNTs more uniformly by repeated ARB cycles depends on their stability or resistance to rupture with subsequent passes.

To study the factors controlling the CNT stability during the ARB process, aluminum CNT metal matrix composite was fabricated and the distribution in terms of their diameters was measured and compared before and after 4 cycles of ARB with 50% reduction in thickness, at each pass. Also to get a better understanding of the mechanical behavior of the composite in terms of their elastic behavior and internal friction, the elastic deflection and vibration damping capacity of the composites fabricated after 5 cycles of ARB, each containing a different CNT concentration at the initial pass, were investigated by cantilever bending test and by the impulse excitation method.

2 Literature review

2.1 Principles of Accumulative Roll Bonding

Accumulative roll bonding (ARB) is a solid state operation in which metals are bonded by rolling at ambient temperature. This process has been examined in a variety of materials such as Al [12], Al alloys [13], IF steel [12] and Al/Steel [14]. Metallurgical bonding is achieved at the interface and this requires that the surfaces be clean and brought to within interatomic distances. The surface cleanliness is difficult to achieve in industrial conditions without a controlled atmosphere. To form the bond, sufficient pressure on the metal strips must be applied and a threshold strain value should be achieved [2]. The schematic illustration of accumulative roll bonding is illustrated in Figure 2-1.

During accumulative roll bonding, multiple layers of metals or alloys are stacked together and then rolled until a sufficient degree of deformation is achieved and a solid-state bond between the original individual metal pieces is formed. By repeating this process on the same sample, large total strains may be achieved in the sample. These stacking and rolling steps are repeated until the desired dimensions or mechanical properties are achieved.

To produce a satisfactory bond by roll bonding, it is essential to remove the contaminating layer on the surface of the metal strips that are to be bonded. This layer may consist of oxides, grease and moisture. Removing this layer from the surface may be done via mechanical or electrical surface treatment [15]. After surface preparation, the strips should be handled carefully to avoid new contamination. The time between rolling and preparation of the sample should also be short in order to avoid significant oxidation of the prepared surface [15]. In general, annealing treatment is performed after rolling in order to increase the interfacial bond strength of the metals since diffusional joining mechanisms are expected to promote a strong metallurgical bond [2].

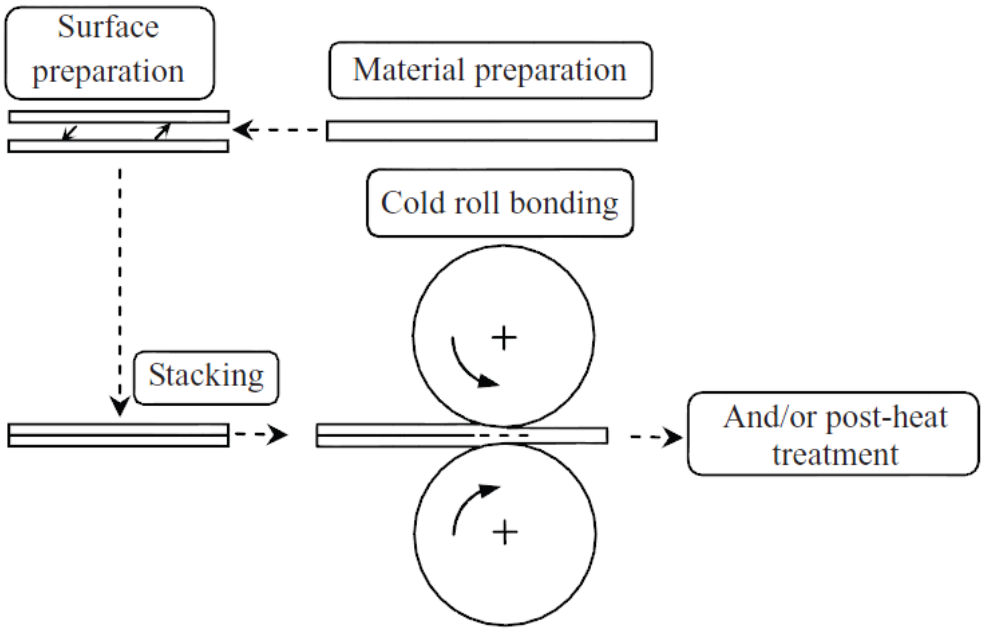

Figure 2-1: Schematic illustration showing principle of cold roll bonding [2].

Figure 2-2 shows the effect of different types of surface preparation on bonding of aluminum composites [2]. The best bonding properties were observed when the surface was degreased followed by scratch brushing. When the procedure is reversed and brushing is followed by degreasing, the bond strength was much lower. In the case of electro-polished surfaces, even an 80% reduction in thickness, bond is not formed, and it has been suggested this is due to the reduction in the number of asperities at the surface.

Scratch brushing is performed for cleaning, but the rough surfaces and asperities that are created while wire brushing also promotes localized shear deformation and breaks more surface oxide films during roll bonding. Therefore, the lowest pressure needed to initiate bonding and the best bond strength is achieved when surface roughening is performed [12, 2].

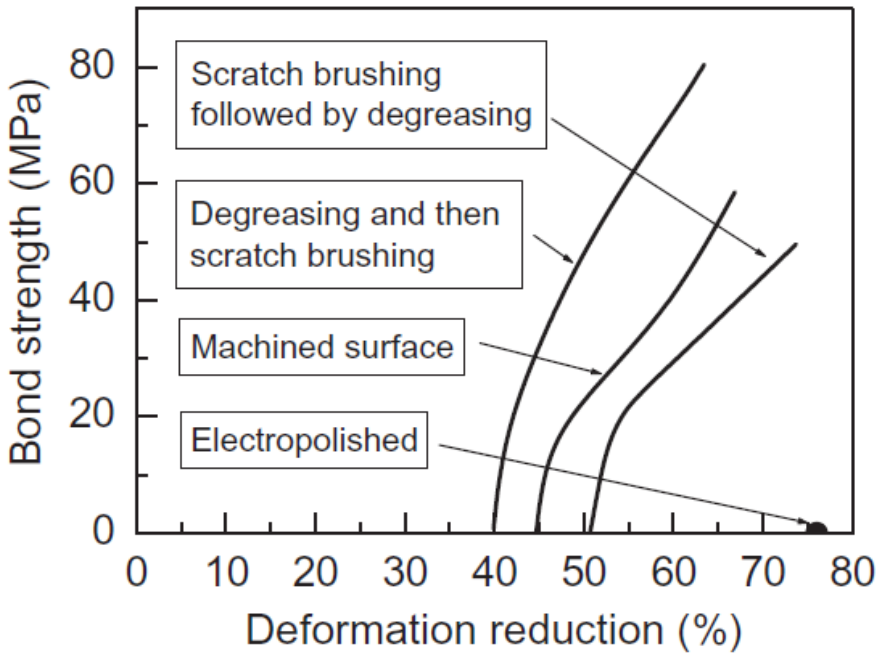

Figure 2-2: Effect of surface preparation on bonding strength during roll bonding of aluminum sheets [2].

2.1.1 Post heat treatment of ARB

It has been shown that heating at low temperatures, before the onset of recovery and recrystallization, for a short time after roll bonding, has increased the strength of the bond. It has been suggested that short-range atomic movements are responsible for improving the strength of the bond. Meaning, if the metallic regions are partially bonded the heat treatment will help complete the bond. Formation of brittle phases at the interface is possible at higher temperatures for some metal matrix composites. Therefore, an optimum annealing temperature should be determined, in order to achieve suitable bond strength and good formability [2,16].

2.1.2 Bonding mechanism

Many attempts have been made during the past decades to understand the mechanism of bonding in cold roll bonding process. It has been found that bond formation consists of 3 steps (Figure 2-3) [17]:

1. Fracture of surface layers resulting from extension of the interface during rolling.

2. Extrusion of underlying surfaces through interfacial cracks from both sides of the interface under the action of the normal roll pressure.

3. Metallic bonding between the freshly created surfaces that approach to within interatomic distances.

The fracture film and the extrusion of the metal through those cracks play a significant role in contact between the metals. Therefore, both the rolling conditions and the material being bonded, control the bond strength and the composite properties.

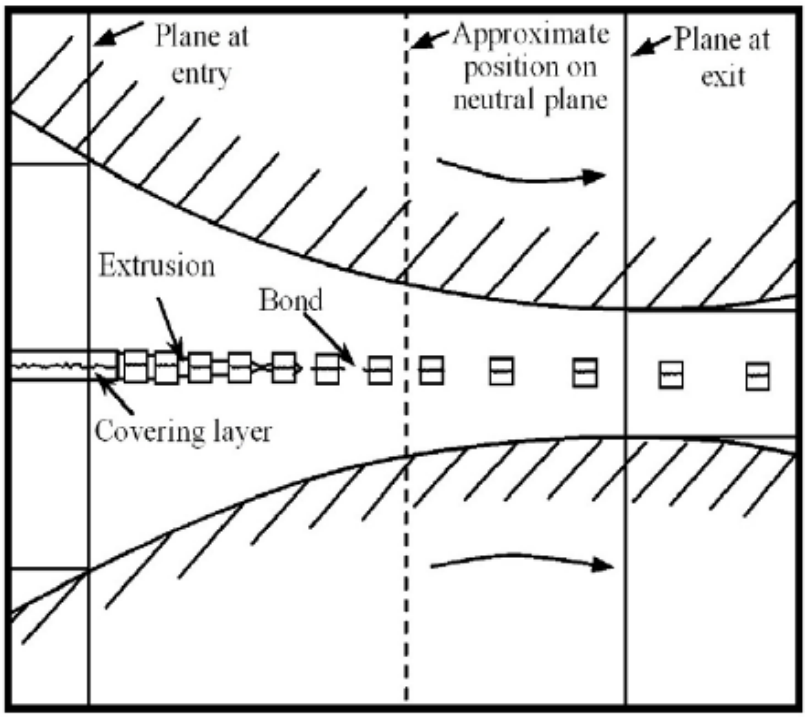

Figure 2- 3: Schematic illustration of fracture and extrusion of surface layer during ARB [2].

2.1.3 Parameters affecting bonding

It has been reported that the roll bonding of metals has been affected by various factors such as the amount of deformation [17], temperature of bonding [17], rolling speed [17], surface conditions [2] and the type of metal [2].

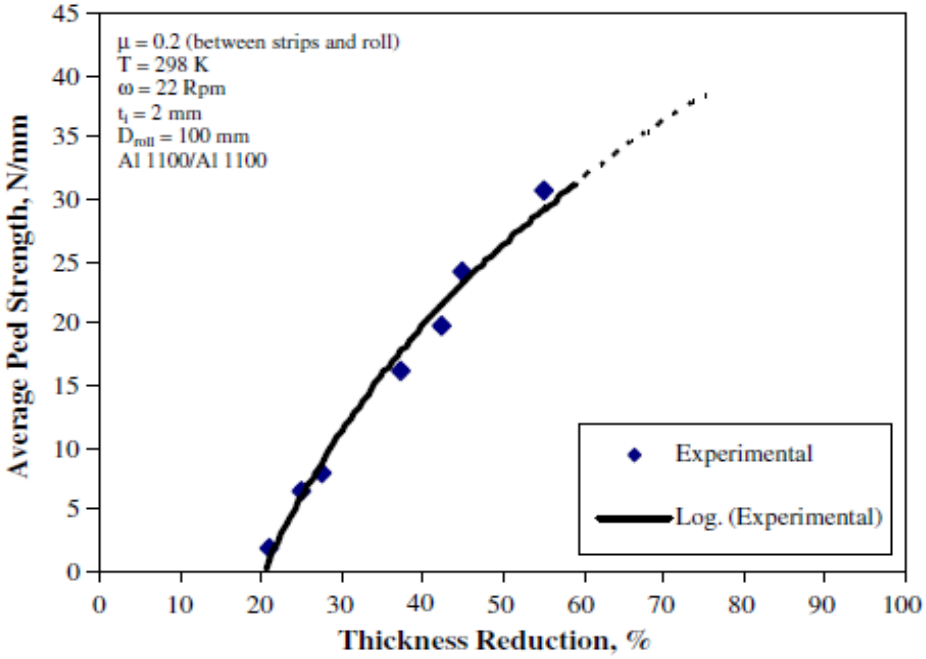

Figure 2-4: Variation of the averages peel strength of two-layer strips of Al/Al versus total thickness reduction [17].

The Figure 2-4 shows the effect of total thickness reduction on the bond strength of two aluminum strips at room temperature. As it is seen, bonding does not occur until a minimum thickness reduction is reached, which is about 21% for aluminum. Also, the bond strength increases when more thickness reduction is achieved. This is due to higher mean pressure and overlapping surface exposure at the interface [2,17]. Figure 2-5 shows the bond strength as a function of deformation reduction for bonds that are produced by cold roll bonding [2]. It is illustrated that the bond is not formed until a minimum threshold deformation is achieved. Beyond this point, the bond strength increases with increasing deformation reduction. The increase in bond strength depends on the strength of the material being deformed [2].

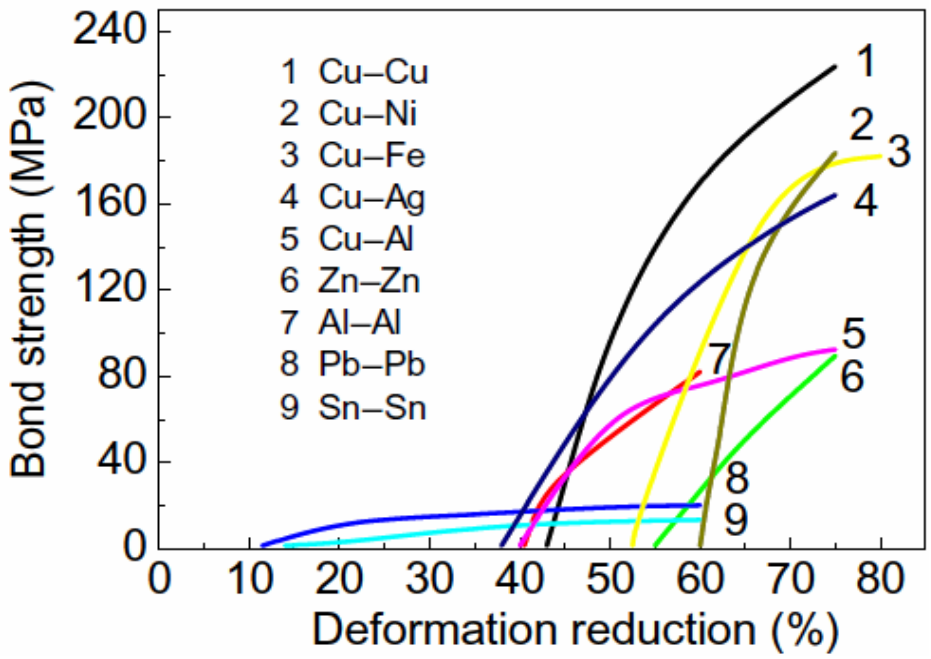

Figure 2-5: Bond strength as function of deformation reduction for bonds formed by cold roll bonding [2].

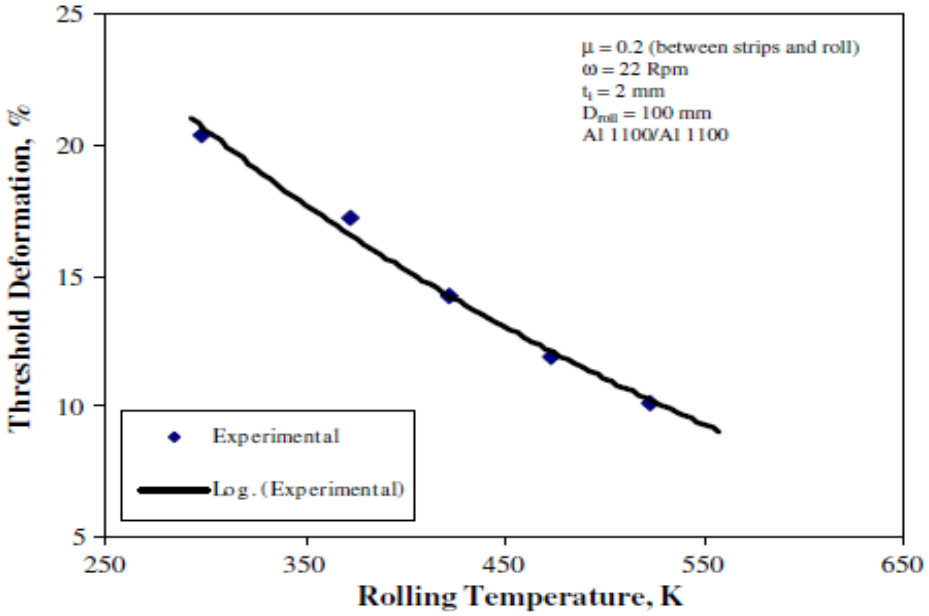

Figure 2-6: Variation of threshold deformation in aluminum-1100 strips versus rolling temperature [17].

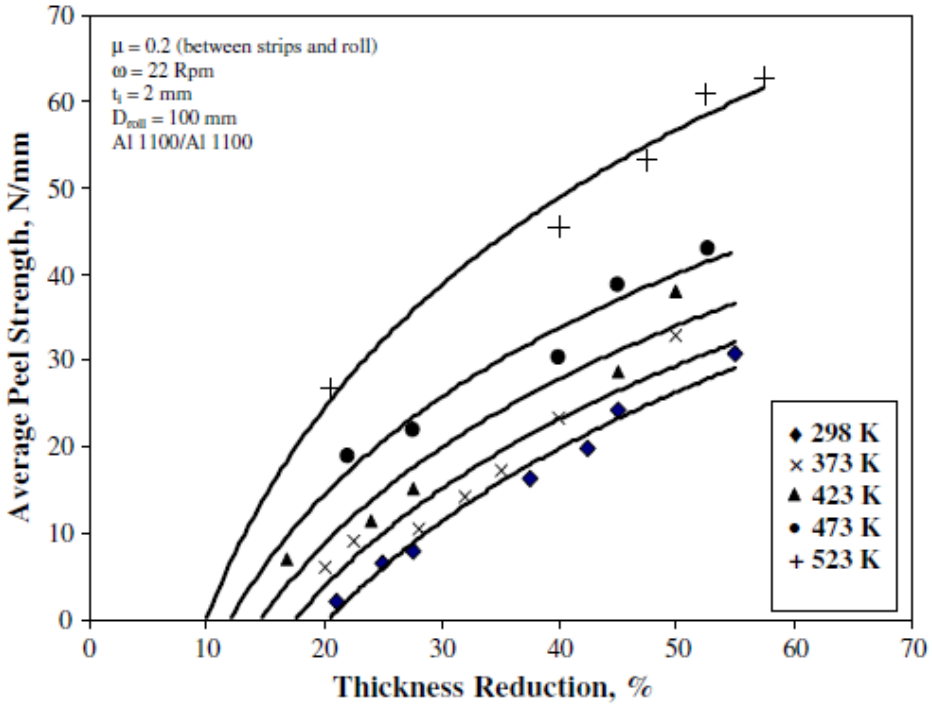

Figure 2-7: Variation of the average peel strength of two-layer strips of Al/Al versus total thickness reduction at different rolling temperatures [17].

Figure 2-6 and 2-7 show the effect of rolling temperature on the strength of the bond at the interface and the minimum thickness reduction required to promote bonding at the interface. These figures illustrate that at a constant threshold deformation, the bond strength improves with increasing temperature. Also, with increasing temperature the minimum reduction required to initiate the bond decreases, since there is a corresponding decrease in the flow stress of metals at higher rolling temperatures. Therefore, the formability of the metal is increased, and more metal may be extruded from the underlying surface through the cracks in the oxide layer compared to that at lower temperatures. This indicates that the bonded area is larger at elevated temperatures [17, 20].

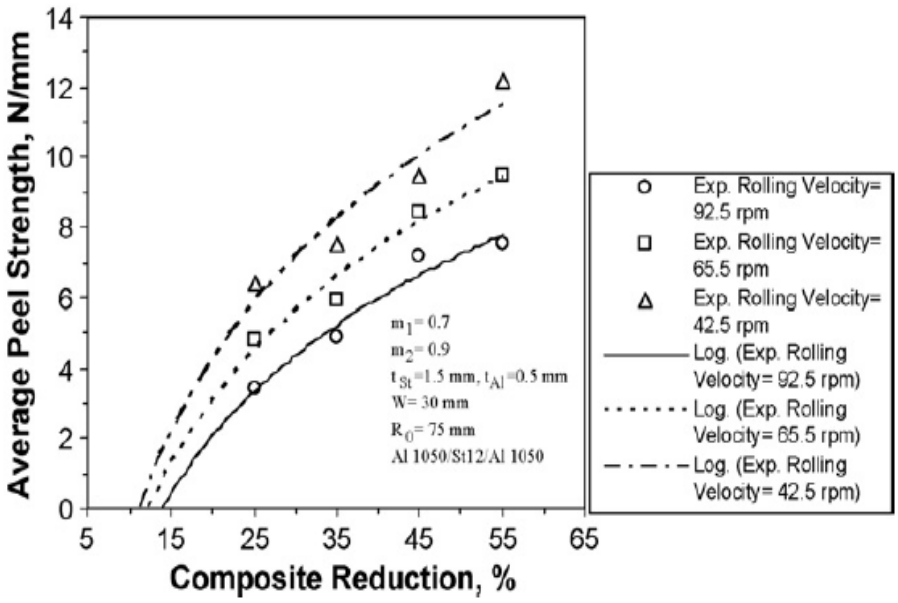

Figure 2-8: Variation of mean bond strength with respect to composite reduction of a sandwich of steel between Aluminum 1050 alloy [20].

Figure 2-8 illustrates the mean bond strength with respect to total composite reduction with increasing the rolling speed. It is shown that the minimum thickness reduction to form the bond increases with increasing rolling speed. Since the total time during which the fresh metal from both sides of the samples are in contact with each other and extruded through the cracks are reduced, the possibility that a bond is created becomes unlikely with increasing the rolling speed. Therefore, more suitable bonding locations i.e. when more of the oxide layer is broken up should be formed on the surface of the material in order to create better bonding. As a result, the minimum threshold deformation is increased at higher rolling speeds [20].

In conclusion, satisfactory bonds are only formed when there is intimate contact between the metals, allowing the two materials to be brought within interatomic separation. To break the surface oxide layer in most alloys, an adequate pressure must be applied in order to provide satisfactory deformation. Scratch brushing of surfaces to be bonded may improve the bond strength. This is one of the critical factors during cold roll bonding since roughness of the surface promotes the formation of asperities, which can more readily be brought into contact at the interface [2].

The bond strength of the metals strips improves by increasing the total thickness reduction. If the temperature of the process is increased, the minimum thickness reduction to achieve bonding will decrease due to the enhancement in the ductility produced by the reduced flow stress. With a constant thickness reduction, the bond strength generally improves with increasing rolling temperature [20, 17].

2.2 Bulk aluminum produced by accumulative roll bonding process

The ARB process has been applied to various kinds of metallic materials such as aluminum alloys and commercially pure aluminum sheets (99.5% purity). For example, Figure 2-9 shows the change in elongation and tensile strength of aluminum sheets of 99.5% pure aluminum. It is interesting to note that both the strength and ductility improve with increasing ARB cycles. For example, Figure 2-9 shows the stress-strain curves obtained for aluminum with up to 8 ARB cycles.

When the stress-strain curves of UFG Al, at constant strain rate, with increasing the number of ARB cycles, are compared, it is revealed that the behavior of these curves are strongly dependent on the number of the cycles. If after 8 cycles the UFG material is compared to the cold rolled material, the strength of the UFG material increases by 80% and the ductility increases by 100% [18].

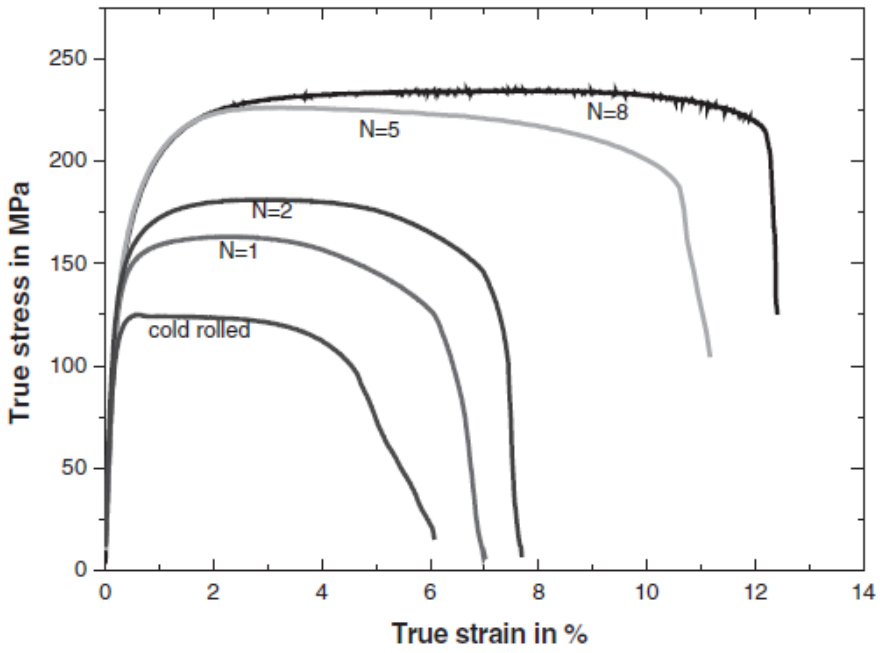

Figure 2-9: True stress vs. true strain for UFG Al at different number of N of ARB passes at constant stain rate of $1x10^{-4}$ S^{-1}[18].

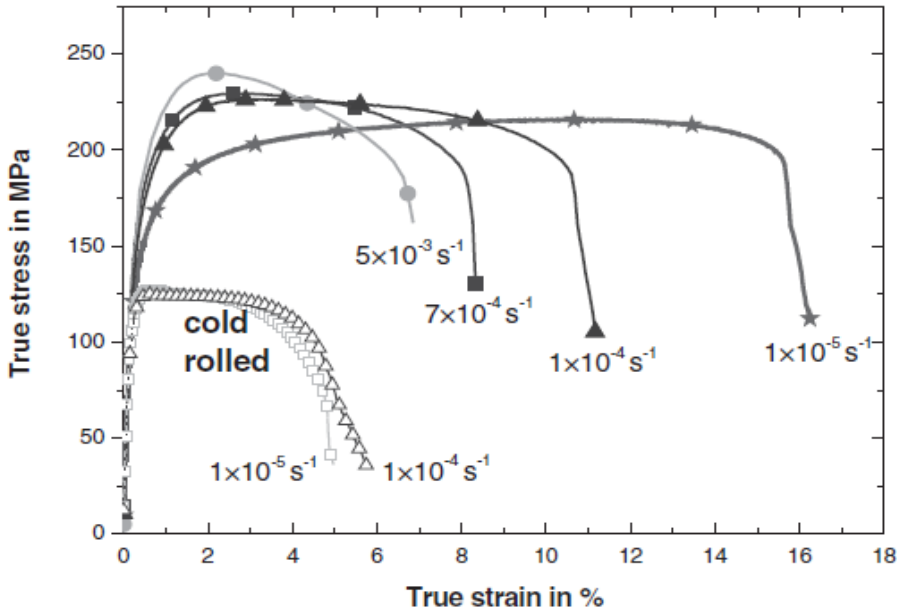

Figure 2-10: True stress vs. true strain for UFG Al after 5 ARB passes and for cold rolled Al tested at different strain rate varying from $1x10^{-5}$ S^{-1} to $5x10^{-3}S^{-1}$[18].

In the case of UFG aluminum, the mechanical properties, such as strength and elongation are strongly dependent on the strain rate. For example, the strain stress curves of UFG aluminum are shown for different strain rates in Figure 2-10. In this case, the material was roll bonded for 5 cycles. The elongation to failure

increases notably with a reduction in the strain rate, and conversely the yield and ultimate strength values increase with strain rate [18].

The increase in maximum elongation of the UFG material may be explained by the increase in misorientation of the grain boundaries. The grain boundaries in nanocrystalline materials act as a source and sink for dislocations. This mechanism is generally more prominent at higher temperatures, however, it is active even at room temperatures in the case of aluminum because the melting point of the material is low and the fine grain size of the specimen promotes the reaction between the dislocations and the grain boundaries [21].

In the case where only a few ARB cycles are performed, the grains are subdivided by cell boundaries and dislocation walls. With increasing the number of ARB cycles, lamellar boundaries are created in rolling direction [22] and the distance between these boundaries decreases, and they will be divided interconnecting boundaries. The sample will be filled with pancake shaped grains along the rolling direction and it is well known that the grain size affects the strength of materials [23].

2.3 Role of shear strain in ultragrain refinement by ARB

Lee et al. [24] were able to show that the minimum grain size corresponds well with the maximum shear strain [24]. The strain distribution through the thickness of an ARB processed sample is shown in Figure 2-11. With increasing the number of cycles, the strain distribution through the thickness of the sample becomes more complicated. An example of this relationship after 4 cycles is given in Figure 2-12. It is observed that the grain size varies depending on the thickness location, which is a result of the increased rate of recrystallizaiton, due to accumulated dislocations where there is larger strain; leading to a smaller grain size [24].

The formation of the ultrafine grains is not only affected by the amount of total strain but also by other factors such as the strain path and the strain gradient introduced during the ARB processes [25]. Other microstructural changes related

to possible grain growth due to the adiabatic temperature rise during rolling may also occur [24].

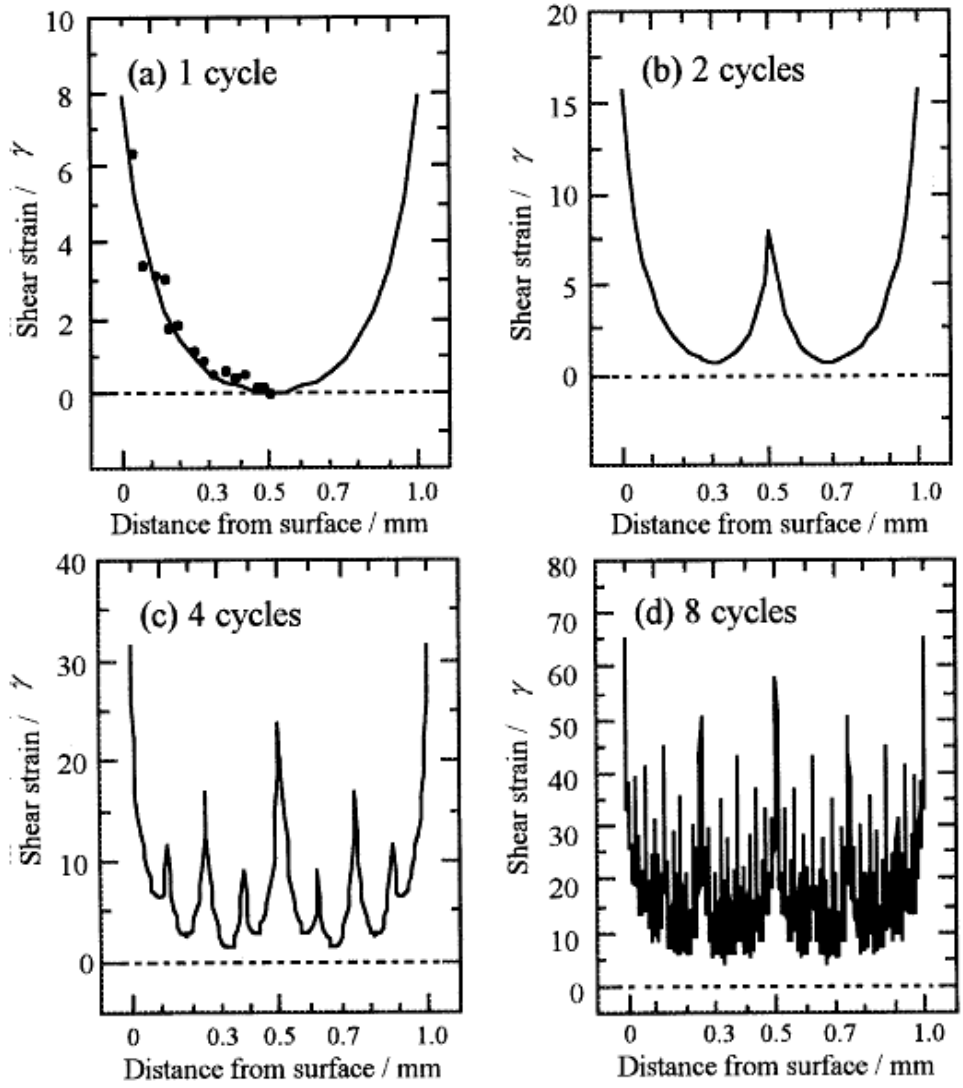

Figure 2-11: Distribution of shear strain through thickness of the 1100 aluminum ARB processed by a) one b) two c) four d) eight cycles [24].

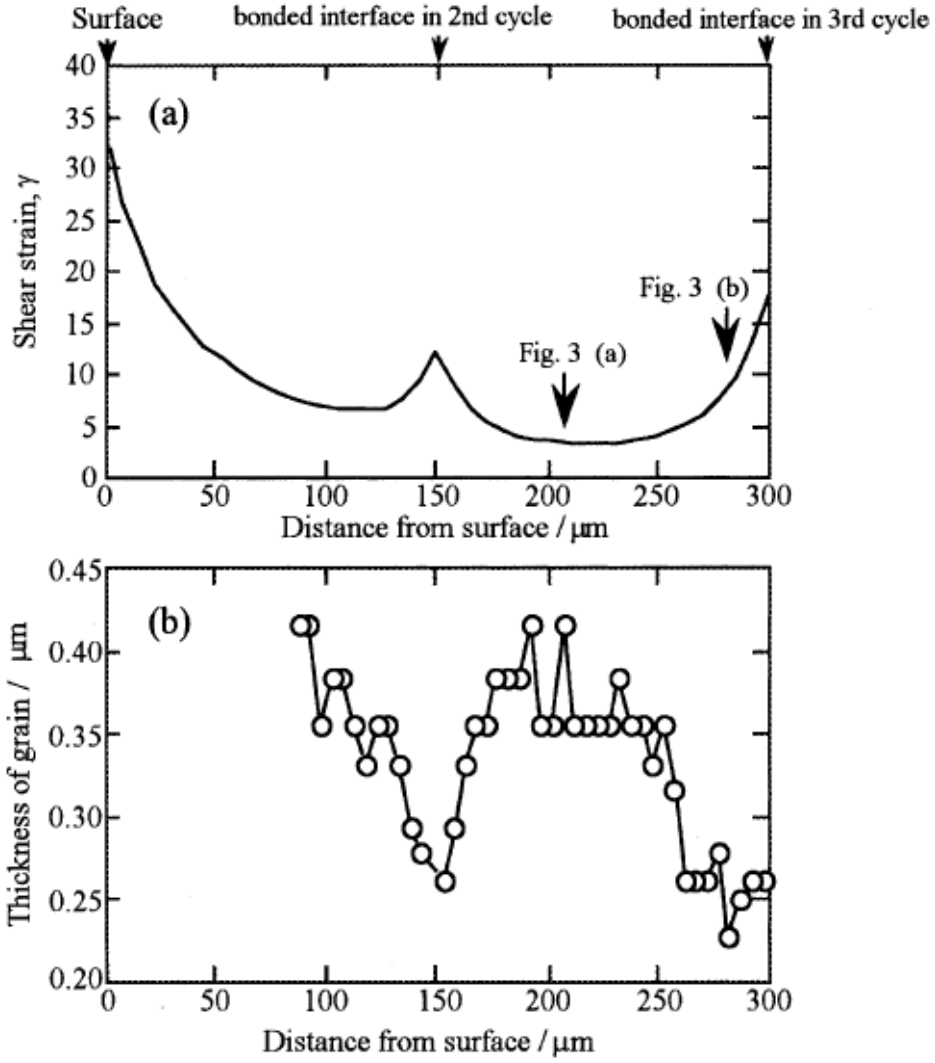

Figure 2-12: Shear strain distribution and grain size distribution in the 1100 Aluminum sheet ARB processes after four cycles [24].

By increasing the number of rolling cycles a subgrained network with low angle grain boundaries or a fine dislocation cell structure is created and subgrain refinement occurs [16,19]. The misorientation of the low angle boundaries progressively increases until a well-defined grain structure consisting of high-angle boundaries is finally established [26].

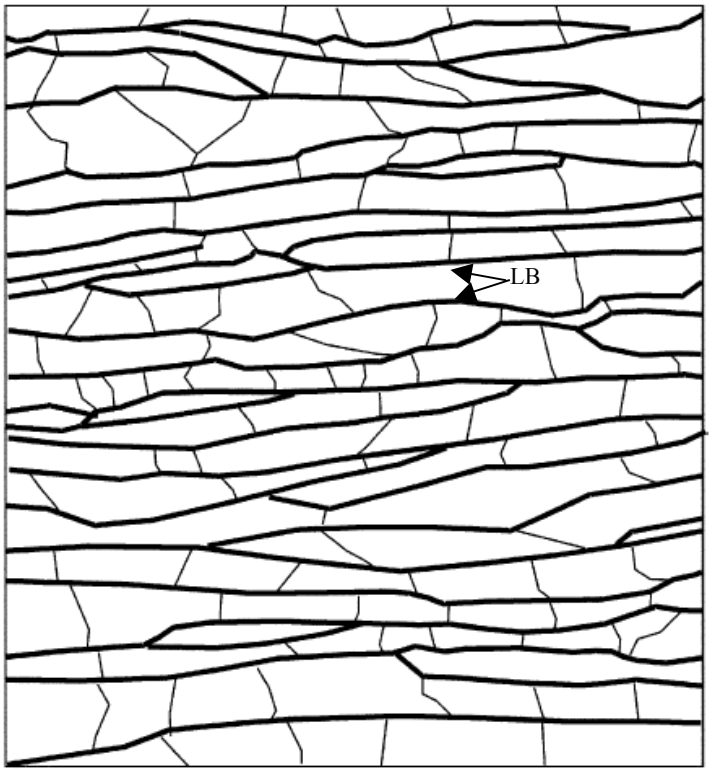

Figure 2-13: Large scale tracing showing lamellar boundaries nearly parallel to the rolling plane and interconnecting boundaries observed in the regions between the lamellar boundaries [26].

The microstructure of a cold rolled commercially pure aluminum is divided to lamellar boundaries, which are parallel to the rolling direction, and a second type of boundaries observed between the lamellar types that are classified as incidental dislocation boundaries or cell boundaries, which arise from statistically stored dislocations, the ones that result from dislocation entanglement. The origin of each type of theses boundaries is different. Lamellar boundaries are classified as geometrically necessary boundaries. These dislocations form as a result of nonuniform strain in the grain; geometrically necessary boundaries are formed to avoid overlap and voids in the material [26]. Lamellar and incidental dislocation boundaries are illustrated in Figure 2-13.

2.4 Variations of the ARB Process

In 2009, Lu et al. [27] used nano-sized SiO_2 particles to enhance bonding during accumulative roll bonding of aluminum alloy 6060. This was done in order to overcome one of the major drawbacks of this severe plastic deformation

method since inadequate bonding can degrade properties. In this experiment, the samples were degreased with acetone and wire brushed. The nano-sized SiO_2 particles were uniformly distributed on the surface of the aluminum strips. The samples were accumulatively rolled for several cycles, with preheating at 300ºC for 3 min. The results showed that with increasing the number of layers up to 16 the strength of the material increases and the elongation of the material decreases. The ultimate tensile strength, yield strength, and elongation of the material are plotted against the number of layers in the sample in Figure 2-14.

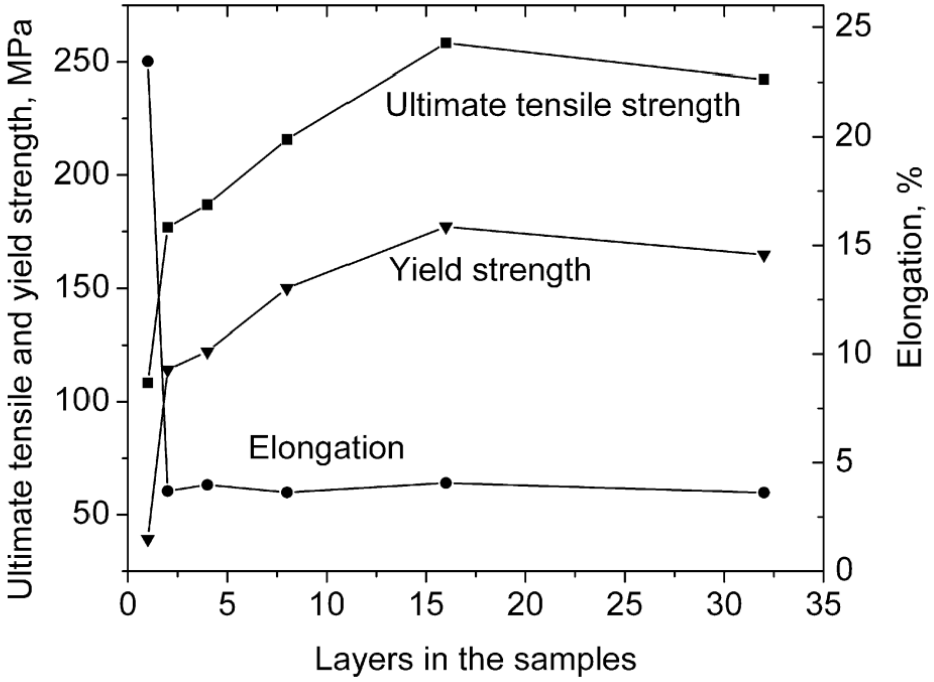

Figure 2-14: Strength and elongation function of layers in the sample [27].

To compare the interfacial bonding behavior, the same experiment was performed without the SiO_2 nano particles. It was observed that an adequate bond could not be formed during the first roll bonding cycle, which shows that the nano particles had a significant role in bond formation. It was suggested that the nano particles improve the bond strength by different mechanisms, by promoting local hardening at the interface and impeding the movement of dislocations that lead to dislocation pile up around the particle. Also, these particles are harder than the material being bonded; therefore, the particles can break up the oxide layer that

exists on the surface of the metal. Although wire brushing has the same effect, it is obvious that with the lag between the wire brushing and roll bonding the oxide layer might form on the surface again. The bond strength of these samples was 2.5 times greater than samples that had no SiO_2 for which the values have been reported before by Krallics and Lenard [28].

Another novel variation of the ARB process has been proposed for the fabrication of metallic foams. These metal foams have some advantages over polymer and ceramic foams including their high melting points and toughness. The manufacturing process of these materials is mostly by melt or powder metallurgy routes. For example, one can produce aluminum powder by blowing TiH_2 particles through the melt, which decompose and release hydrogen at high temperatures that forms bubbles in such high fraction that foam is produced [29].

Kitazono et al. [30] introduced a new method to produce metal foam by accumulative roll bonding. In this method, bulk metal sheets are used as starting materials, which are generally cheaper than metal powder. At the beginning, the two metal strips are stacked together with the appropriate amount of TiH_2 powder between the strips. Then accumulative roll bonding is applied with a 50% reduction performed for several cycles as shown in Figure 2-15.

After performing the ARB process, a high temperature heat treatment was performed on the sample. The temperature profile of the foaming test is illustrated in Figure 2-16. The results of the test showed that the TiH_2 particles were dispersed uniformly in the aluminum matrix.

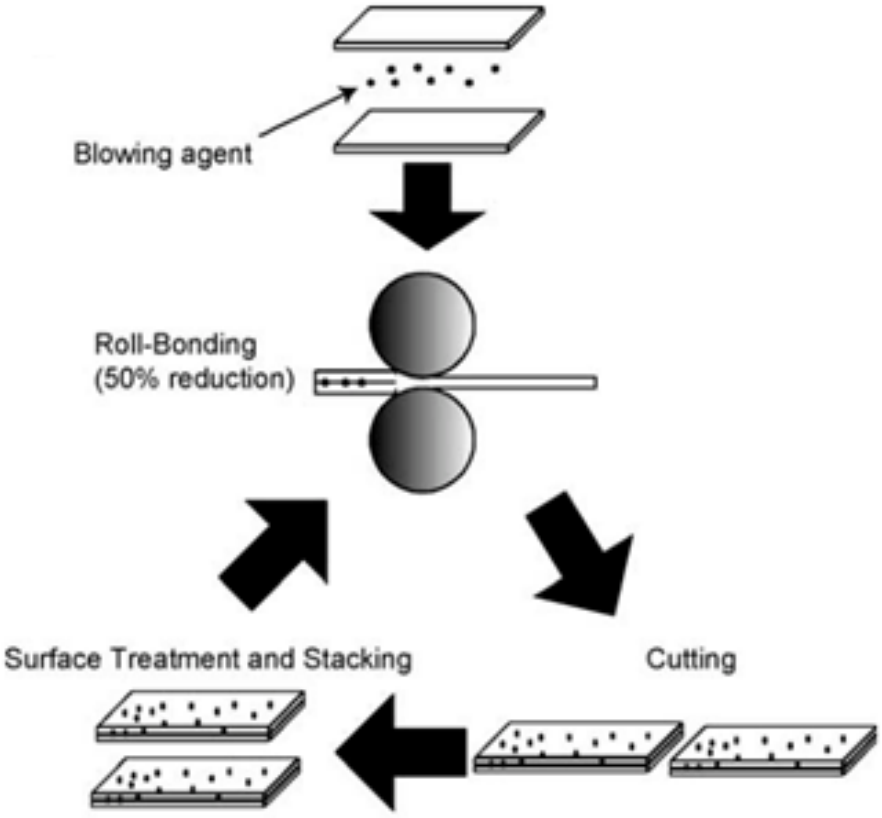

Figure2-15: Schematic illustration of the manufacturing process of perform sheet through ARB process [30].

The porosity of the aluminum foam produced by accumulative roll bonding with TiH_2, increases with increasing foaming temperature. However, at the highest temperatures tested, the porosity decreases again due to gas escaping during annealing. Also, if the specimen is held at high temperatures, the porosity gradually decreases due to cell coalescence. Consequently, the heating rate plays a significant role in the porosity of the material due to hydrogen loss when the heating rates are too low. Figure 2-17 indicates that uniform porosity was achieved in the aluminum matrix.

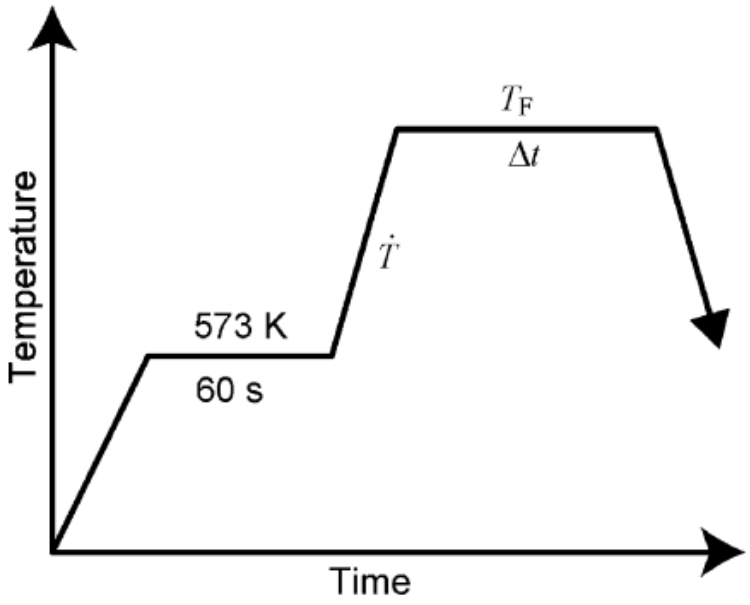

Figure 2-16: Temperature profile during foaming test [30].

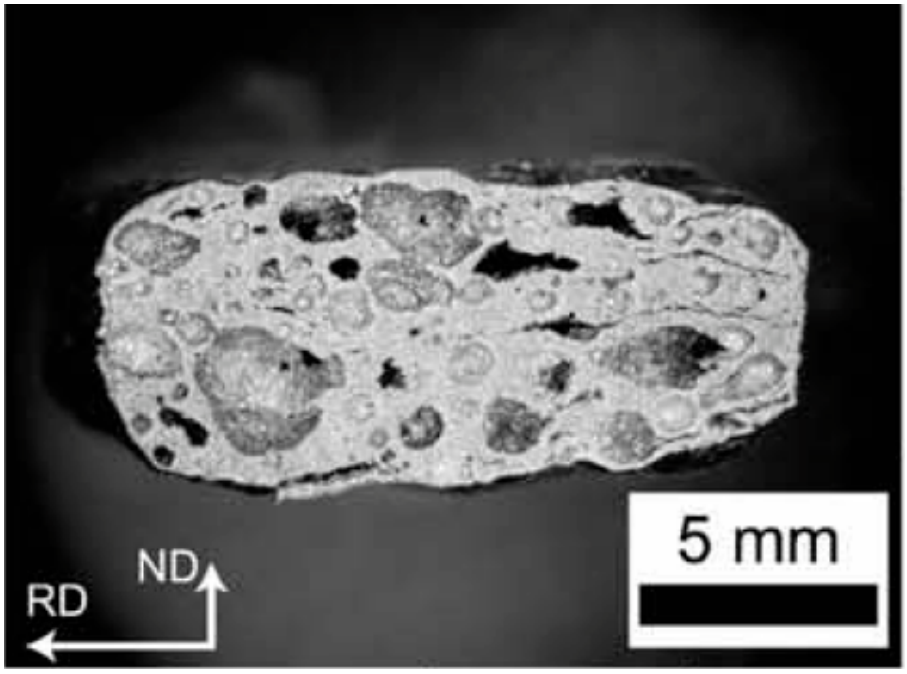

Figure 2-17: Optical microscope image of a foamed Al specimen [30].

During the course of this thesis work, only one other publication emerged which employs a modified ARB approach to produce copper based metal matrix CNT laminate composites [31] in which 10 layers of SWCNT films were sandwiched between 20 layers of Cu thin foils. When samples were annealed at elevated temperatures, mechanical properties were enhanced suggesting that the

diffusion of Cu across the interfaces in the vicinity of the SWCNTs more readily occurs at high temperatures. This leads to improved interfacial bonding between the SWCNT and Cu foils, and the tensile strength of the laminate reached 361 MPa while the Young's modulus reached 132 GPa. This is a significant improvement in comparison with pure Cu, 334 MPa and 117 GPa, which was ARB processed under the same conditions. This improvement in mechanical properties suggests good interfacial adhesion and load transfer between the Cu and SWCNTs.

2.5 Mechanical properties of metal matrix composite (MMC)

Like most composites, metal matrix composite provide unique combinations of properties, such as high stiffness and with no significant change in density, and increased damping capacity.

A metal matrix composite (MMC) provides significant improvement to mechanical properties, such as greater stiffness and higher strength, in comparison with monolithic materials. Therefore, these properties make them a suitable material for a wide range of industries [32,33].

MMCs are generally produced with either particle or fiber reinforcing materials. In particular, particle reinforcement materials have been drawing more scientific attention due to their isotropic properties, cost effectiveness, and simple production methods [32].

Two types of strengthening methods may occur in particle reinforced metal matrix composites: *direct strengthening* and *indirect strengthening*. Direct strengthening happens when load is transferred from the matrix to the reinforcing particles, which are typically higher in stiffness than the matrix. Indirect strengthening results from dislocation strengthening that results from deformation mismatch between the reinforcing particles and the metal matrix [32,33]. The mismatch between the coefficient of thermal expansion of the matrix and the reinforcing particles may be quite significant. Therefore, during the thermal cycles, dislocations form at the interface of the matrix/particle interface and these induced dislocations result in indirect strengthening. A high interfacial area

provides more volume to form these dislocations during contraction upon cooling, thus an increase of reinforcement volume fraction or a decrease in particle size results in higher indirect strengthening [32] due to the localized plastic deformation. Another factor that increases dislocation density in the composite matrix is the mismatch between elastic modulus of particle and matrix [33].

Figure 2-18 demonstrates that the ultimate tensile (UTS) strength, with increasing in volume fraction of the particles with a constant particle size due to higher work hardening rate [32,34]. The lower ductility may be due to attributing to the earlier onset of void nucleation at the reinforcement interfaces [32].

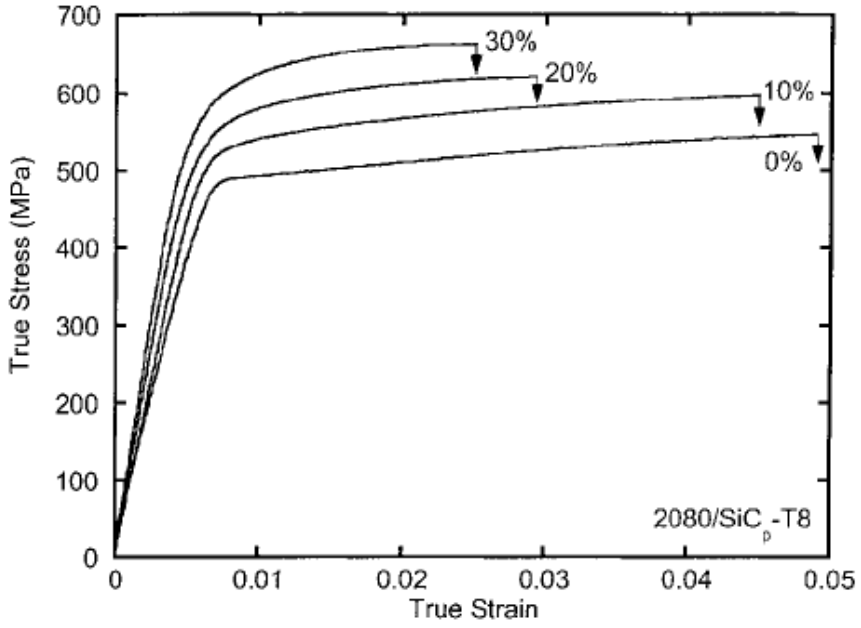

Figure 2-18: Tensile behavior of an Al-Cu-Mg(2080)/SiC-T8 composite with varying volume fraction at constant particle size [32].

Moreover, the yield strength of a reinforced material may decrease in comparison with unreinforced material. This may be due to fracture of the reinforcing particles under the load. These particles do not promote the transfer of load when a fracture exists, the load carrying capacity of the composite decreases and deformation due to microplasicity occurs as a result of the concentration of stress on the corners of the cracked and fractured particles, which may lead to premature yield [32,35]. Therefore when the volume fraction of the particles is constant, fracture of the particles is more likely to happen when the size of the particles is increased. It has been discussed that this is typically why composites

with smaller particle size have better ductility [32]. Consequently at a constant fraction of particles, with larger particle size (in this case larger than 20μm), fracture of the particles are more likely to happen, which leads to lower ductility as was as discussed earlier. (Figure 2-19). Also, dislocation tangles and loops are more likely to happen and the work hardening rate will be higher because the interparticle spacing is lower with larger particles. The work hardening rate of the composite depends on interparticle spacing because at low strains, the dislocations form around the particles and eventually form into a dislocation loops (orawan loop around the particle). That is proportional to the interparticle spacing. Therefore, the rate of work hardening is higher in composites with smaller spacing [34].

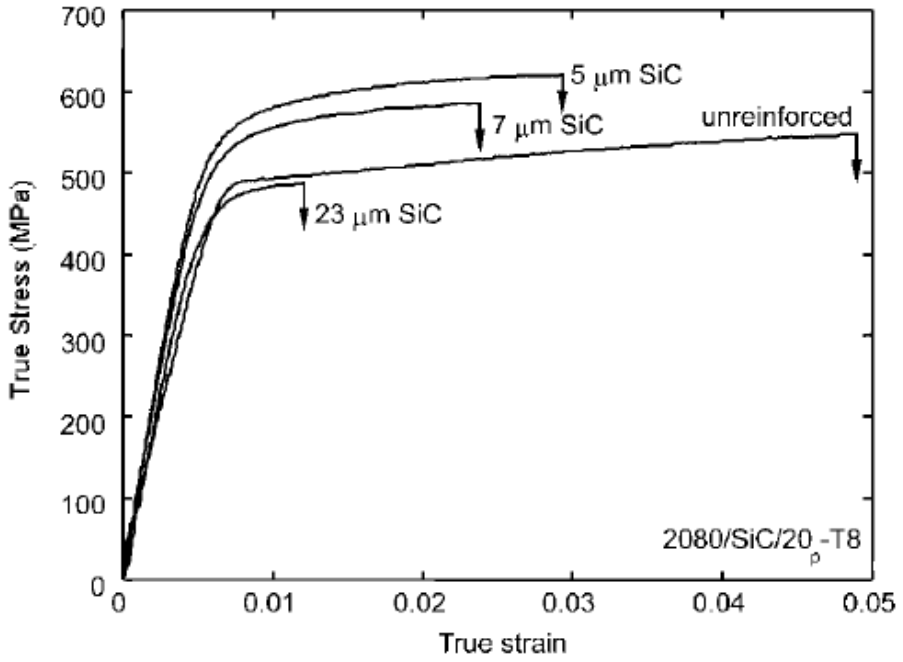

Figure 2-19: Tensile behavior of an Al-Cu-Mg (2080)/SiC-T8 composite with varying particle size at constant volume fraction of 20% [32]**.**

2.6 Carbon nanotube reinforced metal matrix composites

Production of carbon nanotube (CNT) reinforced metal matrix composites (MMCs) has become the focus of many research studies. These composites offer high specific strength as well as exceptional thermal and electrical characteristics.

For example, measurements have shown that CNTs have extraordinary mechanical properties. The Young's modulus of CNTs is reported to be about 1.8 TPa and their bending strength is about 14.2 GPa in conjunction with their low density (1.35g/cm^3) [36]. This property makes CNTs an ideal reinforcing particle for manufacturing of MMCs because of their high specific strength and stiffness.

In comparison with studies on CNTs alone, the amount of research on CNT reinforced metal matrix composites is rather limited. This is due to the complexity of interfacial reactions between the CNTs and the matrix. In order for the CNTs to work as an effective reinforcement to improve the mechanical properties of the composite, the main critical issues that must be considered are CNT distribution in the metal matrix and interfacial bonding of the CNT and matrix as well as any chemical reactions between the matrix and the CNTs. In addition, one also needs to consider CNT agglomeration since this influences load transfer from the matrix to the particles and interfacial bonding between CNTs and the matrix [5]. A variety of process techniques has been applied to prepare carbon nanotube reinforced metal matrix (MM-CNT).

The most popular technique used for manufacturing MM-CNT is powder metallurgy [37]. However, other techniques such as melting, solidification and electro-deposition of thin composite coatings to produce one-dimensional composites have also been successfully employed.

The powder metallurgy technique is a promising method to fabricate MM-CNT. The process steps consist of mixing the CNT with metal powder by mechanical alloying, followed by consolidation by compaction and sintering, then hot or cold isostatic pressing (or plasma sintering), followed by rolling or extrusion, such as equal-channel angular processing. Most of the studies on Al-CNT are carried out by these methods [38].

Another technique to produce MMC is melting and solidification. Since this process is performed at high temperatures, it may cause damage to the CNTs and cause reaction between the CNT and the matrix. Therefore, this route is commonly used for fabricating metal matrix composites with low melting temperature matrix [37]. This is a particular problem with CNTs since their

exceptionally high surface area promotes rapid degradation during any reaction at high temperatures. Some other novel procedures such as accumulative roll bonding [5, 31] and friction stir welding [39, 40] have been used to produce MM-CNT composites.

As was mentioned before, Lei et al. [31], produced laminated Cu-CNT composites which resulted in improvement of mechanical properties.

Lahiri et al. [5] used the sandwich method to produce Al/CNT composites by joining 4 layers of Al and layers of CNTs. The elastic modulus increased by 59% with a 2vol% CNT addition in aluminum. This process has the potential to become a popular technique due to its ease of processing.

Since the goal of adding CNT to the metal matrix is to increase tensile strength and elastic modulus of the composites, the addition of CNT allows the load applied to the matrix to be transferred to the CNT at the interfacial regions. Therefore, the main issues in mechanical properties of metal matrix-CNT composites are uniform dispersion during processing to achieve a homogenous distribution in the composite, and control of interfacial reactions to provide good bonding between the CNTs and the matrix.

Reaction of the matrix and the carbon fibers may lead to the formation of carbide at the interfacial layer, which affects the stress transformed to the fibers. Debonding may happen when the matrix or the interface fails under the stress. If the stress exceeds the shear strength of the carbides, fracture may occur, leading to CNT pull out [41]. Consequently, the different carbides formed at the interface may lead to different mechanical properties in the composite due to the different shear strengths of these carbides. Other factors such as porosity of the composite, agglomeration of CNTs, and wavy shape of the CNTs that are often resulting from their high aspect ratios, are also important in mechanical properties of the composites [37].

Carbide formation may be controlled by many factors such as temperature of the process or the chemistry of the matrix. Also, defects in the CNT may lead to carbide formation as they provide sites for chemical reactions to occur [37,42]. The solubility limit of carbon is less than 0.1 ppm at 750 ºC; hence, the solubility

of carbon in aluminum at room temperature can be neglected [43]. Chunfeng et al. [44] found no evidence of the CNTs in the Al 2024 alloy matrix. When it was heated up to 1073 K, XRD results showed that CNTs were fully converted to Al_4C_3. This indicates that the formation of aluminum carbide at room temperature less likely to take place, and a fabrication process at ambient temperature will yield composites with more desirable mechanical properties.

The fact that CNTs have a very large surface area of up to $200m^2g^{-1}$ makes uniform dispersion of CNTs a challenge for production of CNT reinforced composites due to the Van der Waals forces between them, and so CNTs tend to form clusters [37,45]. This agglomeration leads to a heterogeneous weight fraction of CNTs, and since this is a very important factor for the elastic modulus and strength of the composites, any agglomeration will severely degrade properties.

Another factor that significantly affects the overall mechanical properties of the composites is the CNT orientation in the matrix. The best form of orientation of CNTs in the metal matrix to achieve homogenous properties is randomly distributed fibers. For example, The Voigt-Reuss [37] model suggests that for randomly oriented CNT composites, the elastic modulus is given by:

$$E = \frac{3}{8}E_{\parallel} + \frac{5}{8}E_{\perp} \qquad \text{(Equation 2-1)}$$

where $E_{\parallel} = V_f E_f + (1 - V_F)E_m$ is the longitudinal modulus and $E_{\perp} = \frac{E_f E_m}{E_f(1 - V_f) + E_m V_f}$ is the transverse modulus . E stands for elastic modulus, V for volume fraction; m corresponds to matrix and f to fiber (CNT).

2.7 Al-CNT composites

There have been different attempts to overcome the problem of CNT agglomeration and formation of dense bundles, to achieve a homogenous distribution of CNTs in a metal matrix by solid and liquid state processing routes. Since CNTs may form into Al_4C_3 carbide at high temperatures, many

thermomechanical processes cause deterioration of the CNTs or composite mechanical properties.

Esawi et al. [9] produced Al-CNT composite using ball milling followed by hot extrusion to produce 2wt% MWCNT in aluminum powder. This process has the advantage of strain hardening the aluminum powders, which may improve implication of the final properties of the composite. Choi et al. [38] observed that grain size is dependent on the milling time and conditions. Moreover, they showed that ball milling is an effective way to disperse the CNTs uniformly in aluminum powder and the properties were improved due to better dispersion of CNTs and strain hardening of the powders [9, 38].

Ewaski et al. [9] found a 21% tensile strength improvement in comparison with pure aluminum that was ball milled for 3 hours and extruded at 500º C. However, there are concerns about possible damage to the structure of the CNTs [9, 38]. Also possible problems may occur from aluminum matrix/CNT interfacial reactions leading to formation of undesirable Al_4C_3 since high temperature processing after ball milling is required in order to consolidate the composite and sinter the powder with the CNTs. During ball milling or explosive consolidation to disperse or blend the powders, the temperature rises significantly, which reduces the effect of reinforcement of CNTs in the composite.

When concentrations are increased, agglomeration of the CNTs may occur and result in reduction rather than an improvement in the mechanical properties. For example, Salas et al. [6] produced Al-5vol% CNT and Al-2vol% CNT using explosive consolidation. A composite with 2vol.% MWCNT showed a decrease in hardness of about 2.5% compared to the shock wave consolidated aluminum, while a further increase in MWCNT concentration to 5 vol.% exhibited a further hardness decrease of 18%. This was argued to be a result of weakening of the matrix/CNT interface bonding during agglomeration.

He et al. [46] were the first to synthesize Al-CNT composites by growing the CNTs directly on aluminum powder using chemical vapor deposition (CVD) method and comparing them with pure aluminum. Using CVD, a homogenous dispersion of CNTs within the Al powder was achieved, and consequently these

composites showed extreme enhancement in mechanical properties. Another advantage of this method is the length and size of the CNTs, which may also be controlled. Therefore, they were able to produce Al-5wt% CNT composites that are fully dense at 96%. The hardness of the CNT-Al composite was 4.3 times higher than pure aluminum. Lahiri et al. [5] utilized the ARB process to produce laminated Al-CNT composites, this technique has also been used to fabricate Cu/CNT laminated composite by combining cold roll bonding and annealing [31]. The tensile strength and the Young's modulus of the composite were 361 MPa and 132 GPa respectively, which showed significant improvement in comparison to pure Cu. The ARB process results in grain refinement, CNT alignment, and better dispersion of the CNTs in the matrix. They achieved a 59% increase in elastic modulus with a Al-2vol.% CNT composite. A Al-9.5vol.% CNT was found to have a 250% higher tensile strength in comparison to pure Al.

In summary, concentration is not the only factor that plays a major role in controlling the mechanical properties of Al-CNT composites. The homogeneity of the CNT distribution and strong bonding with the matrix also has a significant impact on these properties.

2.8 Bibliography

[1] Y. Saito, H. Utsunomiya, N. Tsuji, T. Sakai, Acta Metallurgica 47 (1999) 579-583.

[2] L. Li, K. Nagai, F. Yin, Science and Technology of Advanced Materials 9 (2008) 023001.

[3] N. Tsuji, Y. Saito, S.H. Lee, Y. Minamino, Advanced Engineering Materials 5 (2003) 338-344.

[4] N. Toru, M. Akira, F. Shigeru, S. Shuchi, B. Junichi, S. MAsayuki, Materials Transactions 45 (2004) 602-604.

[5] D. Lahiri, S.R. Bakshi, a K. Keshri, Y. Liu, A. Agarwal, Materials Science and Engineering: A 523 (2009) 263-270.

[6] W. Salas, N.G. Alba-Baena, L.E. Murr, Metallurgical and Materials Transactions A 38 (2007) 2928-2935.

[7] P. Quang, Y. Jeong, S. Yoon, S. Hong, H. Kim, Journal of Materials Processing Technology 187-188 (2007) 318-320.

[8] K. Morsi, A. Esawi, Journal of Materials Science 42 (2007) 4954-4959.

[9] A.M.K. Esawi, K. Morsi, A. Sayed, a A. Gawad, P. Borah, Materials Science and Engineering: A 508 (2009) 167-173.

[10] J. Suhr, N. Koratkar, P. Keblinski, P. Ajayan, Nature Materials 4 (2005) 134-137.

[11] D. Lahiri, S.R. Bakshi, a K. Keshri, Y. Liu, A. Agarwal, Materials Science and Engineering: A 523 (2009) 263-270.

[12] S.Y.M. Tsuji, Ito Y, Scripta Materialia 47 (2002) 893-899.

[13] N. Tsuji, T. Iwata, M. Sato, S. Fujimoto, Y. Minamino, Science and Technology of Advanced Materials 5 (2004) 173-180.

[14] H. Manesh, A. Taheri, Journal of Alloys and Compounds 361 (2003) 138-143.

[15] M. Eizadjou, H. Danesh Manesh, K. Janghorban, Materials & Design 30 (2009) 4156-4161.

[16] N. Tsuji, T. Toyoda, Y. Minamino, Y. Koizumi, T. Yamane, M. Komatsu, M. Kiritani, Materials Science and Engineering A 350 (2003) 108-116.

[17] M. Eizadjou, H. Daneshmanesh, K. Janghorban, Materials & Design 29 (2008) 909-913.

[18] H.W. Höppel, J. May, M. Göken, Advanced Engineering Materials 6 (2004) 781-784.

[19] G.E. Dieter, Mechanical Metallurgy, Third Edition, 1976.

[20] H.D. Manesh, H.S. Shahabi, Journal of Alloys and Compounds 476 (2009) 292-299.

[21] W. Cao, a Godfrey, W. Liu, Q. Liu, Materials Science and Engineering A 360 (2003) 420-425.

[22] N. Hansen, R.F. Mehl, A. Medalist, Metallurgical and Materials Transactions A 32 (2001) 2917-2935.

[23] H. Kim, S. Kang, N. Tsuji, Y. Minamino, Acta Materialia 53 (2005) 1737-1749.

[24] S. Lee,Y. Saito, N. Tsuji, H. Utsunomiya, T. Sakai, Scripta Materialia 46 (2002) 281-285.

[25] Y. Iwahashi, Z. Horita, M. Nemoto and T.G. Langdon, Acta Materialia 46 (1998) 3317-3331.

[26] N. Hansen, X. Huang, R. Ueji, N. Tsuji, Materials Science and Engineering A 387-389 (2004) 191-194.

[27] C. Lu, K. Tieu, D. Wexler, Journal of Materials Processing Technology 209 (2009) 4830-4834.

[28] G. Krallics, J. Lenard, Journal of Materials Processing Technology 152 (2004) 154-161.

[29] S. Akiyama, H. Ueno, K. Imagawa, A. Kitahara, S. Nagata, M. K, patent number 4713277, 1987.

[30] K. Kitazono, E. Sato, K. Kuribayashi, Scripta Materialia 50 (2004) 495-498.

[31] Y.H. Li, W. Housten, Y. Zhao, Y.Q. Zhu, Nanotechnology 18 (2007) 205607.

[32] N. Chawla, Y.L. Shen, Advanced Engineering Materials 3 (2001) 357-370.

[33] L.H. Dai, Z. Ling, Y.L. Bai, Composites Science and Technology 61 (2001) 1057-1063.

[34] M. Manoharan, J.J. Lewandowski, Materials Science and Engineering A 150 (1991) 179-186.

[35] T. Doel, Composites Part A: Applied Science and Manufacturing 27 (1996) 655-665.

[36] Y. Zhang, Y. Xue, L. Sinian, H. Jin, J. Haun, 488-489 (2005) 897-900.

[37] S.R. Bakshi, D. Lahiri, A. Agarwal, International Materials Reviews 55 (2010) 41-64.

[38] H. Choi, J. Shin, B. Min, J. Park, Materials Science 24 (2009) 2610-2616.

[39] Y. Morisada, H. Fujii, T. Nagaoka, M. Fukusumi, Materials Science and Engineering: A 419 (2006) 344-348.

[40] L.B. Johannes, L.L. Yowell, E. Sosa, S. Arepalli, R.S. Mishra, Nanotechnology 17 (2006) 3081-3084.

[41] J. Coleman, U. Khan, W. Blau, Y. Gunko, Carbon 44 (2006) 1624-1652.

[42] L. Ci, Z. Ryu, N. Jinphillipp, M. Ruhle, Acta Materialia 54 (2006) 5367-5375.

[43] C.J. Simensen, Metallurgical Transactions A 20 (1989) 191-191.

[44] D. Chunfeng, Z. Xuexi, W. Dezun, Materials Letters 61 (2007) 904-907.

[45] W. Salas, N.G. Alba-Baena, L.E. Murr, Metallurgical and Materials Transactions A 38 (2007) 2928-2935.

[46] C. He, N. Zhao, C. Shi, X. Du, J. Li, H. Li, Q. Cui, Advanced Materials 19 (2007) 1128-1132.

3 Fabrication of an aluminum-carbon nanotube metal matrix composite by accumulative roll bonding[1]

3.1 Introduction

Accumulative roll bonding was developed by Saito et al. [1] as a severe plastic deformation technique for refining the grain size of an alloy. In this process multiple layers of metals or alloys are stacked together and then rolled until a sufficient degree of deformation is achieved and a solid state bond between the original individual metal pieces is formed. To form the bond, sufficient pressure on the metal strips should be applied and a threshold strain value should be achieved [2].

This deformation facilitates grain refinement to the nanocrystalline range, and therefore a high degree of strengthening can be achieved using ARB in various kinds of steels and aluminum alloys [3-5]. Laminated composites of alternating metal layers may be fabricated by the ARB process, and this has been demonstrated with foils of Ni and Zr [6], Al and Ni [7], as well as Ni, Ti and Zr [8]. In some cases it was possible to produce a laminated sheet with nanocrystalline or even amorphous microstructure [6, 8]. The total reduction applied on the material may be limited due to embrittlement with increasing work hardening, however ductile materials can be roll bonded to exceptionally high total strains [3].

A variation of the roll bonding process has been developed in which a nanoscale powder reinforcing material is dispersed between the sheets prior to rolling, with the aim of producing a layer of metal matrix composite material at the interface. The process is similar to sheath-rolling which has been discussed elsewhere [9], however it does not require reheating or vacuum encapsulation of the sheets. Fabrication of composites by roll bonding has been demonstrated using Al sheets and SiO_2 particles [10], Cu foils and single walled carbon nanotubes

[1] Portions of this chapter were published in Journal of Materials Science, Volume 46, Number 2, 409-415

(CNTs) [11], and Al foils with multiwalled CNTs [12]. In all cases the layered composites exhibited both increased strength and stiffness due to the exceptional properties of the CNTs [13-14]. These structural enhancements may be realized in a metal matrix composite and potentially also offer improved electrical and thermal properties [15-17].

The fabrication steps involved are summarized in Figure 3-1. This process has the advantage of increasing the strength of the matrix material via grain refinement, and has the potential to achieve high concentrations of CNT material in the composite since the process has the potential to be repeated for several passes by changing the parameters of the process. It should also been noted that it has been proposed that reinforcing fibers are dispersed and preferentially aligned in the rolling direction during roll bonding of CNT metal matrix composites [11,12]. Also the rate of entanglement in the CNT base material may be reduced during fabrication using this process, particularly with increased strains during repeated rolling operations.

Although a great deal of success has been achieved in synthesizing polymer-CNT composites, producing metal matrix CNT composites is rather challenging. However, some techniques have included hot extrusion, equal channel angular pressing, shockwave consolidation, and mechanical alloying [18-20]. The use of CNTs as a reinforcement has been shown to provide improved properties in various metal matrix composites [21-23], however a number of challenges need to be considered during synthesis. For example, the processing route may result in damage of the nanotube structure, poor interfacial bonding between CNTs and metal matrix, or agglomeration of the CNTs [24]. Sintering of metal powders with CNTs at high temperature may promote chemical reaction of nanotubes with the surrounding matrix, although this may be detrimental to the properties of the CNT [25]. Although possible damage to the CNTs has been suggested during roll bonding of Al-CNT composite [12], the factors controlling the CNT stability during the process have never been examined. This is a particular concern since potential to distribute the CNTs more uniformly by

repeated ARB cycles depends on their stability or resistance to rupture with subsequent passes, and this issue is addressed in this chapter.

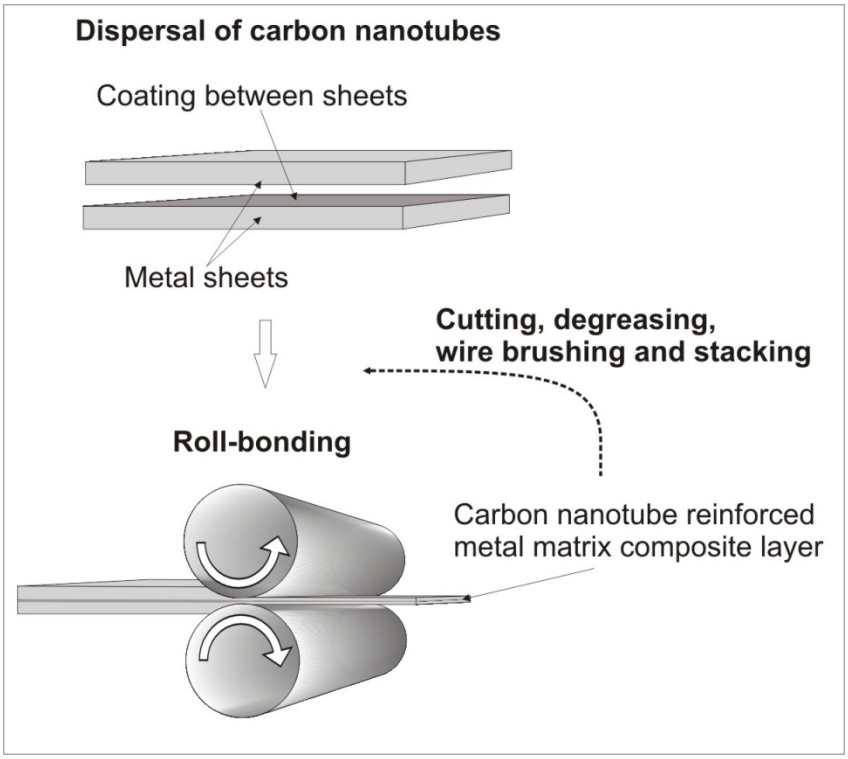

Figure 3-1: Schematic illustration of the composite fabrication process via accumulative roll bonding.

3.2 Experimental methods

The sheet material used during roll bonding was a commercially pure aluminum alloy (AA1100) with a composition of Al-0.51Fe-0.13Cu-0.08Si-0.03Mn. The as-received aluminum consisted of a fully annealed microstructure with an equiaxed average grain size of 52 μm, and was cut into 150 x 25 x 1.4 mm strips. Multiwalled CNTs were ultrasonically agitated in 2-propanol, and then heated in order to evaporate the alcohol and obtain a highly concentrated suspension of CNTs. After degreasing the aluminum and wire brushing the surfaces, the sheets were coated once only before the initial pass using a spatula,, with the concentrated CNT suspension and allowed to dry. The sheets were then stacked together making a 2.8 mm thick sandwich that was accumulatively roll bonded 4 times at room temperature with intermediate degreasing and wire

brushing as indicated in Figure 3-1. The diameter of the rollers was 100 mm, the rolling speed was 75 rpm, and the thickness reduction was 50% during each pass. It should be noted that the aluminum sheets were only coated with CNT material once in order to determine the influence of mechanical loading on nanotubes all exposed to the same number of rolling cycles. In addition, when fewer than 4 passes were applied, in adequate bonding resulted in delimitation of the samples, and when more than 5 passes are applied cracking at the edges made it difficult to subsequently repeat roll bonding.

TEM was used to study the microstructure of the metal matrix composite. The TEM samples were prepared from 3 mm disks which were punched out from the plan view of the sheet and mechanically thinned. These were then electropolished using a solution of 25 vol.% of HNO_3 and 75 vol.% of methanol at a temperature of -35ºC and voltage of 12 V, and examined using a JEOL 2010 microscope operating at 200 kV. Samples which were observed along the transverse plane of the sheet were sectioned using electrical discharge machining before electropolishing.

3.3 Results and discussion

3.3.1 Aluminum matrix and CNT microstructures

Figure 3-2 shows the morphology of the as-received CNTs which ranged in diameter from 10 to 70 nm, and a nominal axial length of 10 to 20 μm. Due to their length and morphology, the as-received CNT material was highly entangled. The microstructure of the CNTs and matrix grains in the composite material following 4 rolling passes are shown in Figure 3-3 & 3-4. The repeated rolling cycles produced an ultrafine grained matrix consisting of high-angle boundaries with grain sizes ranging from 100 to 500 nm in the rolling direction. However in the normal direction (ND) of the sheet, the grains with thicknesses of <100 nm could readily be observed, with an average grain thickness after four cycles of 109 nm see Figure 3-4b. The grains were not completely equiaxed and exhibited some elongation in the rolling direction.

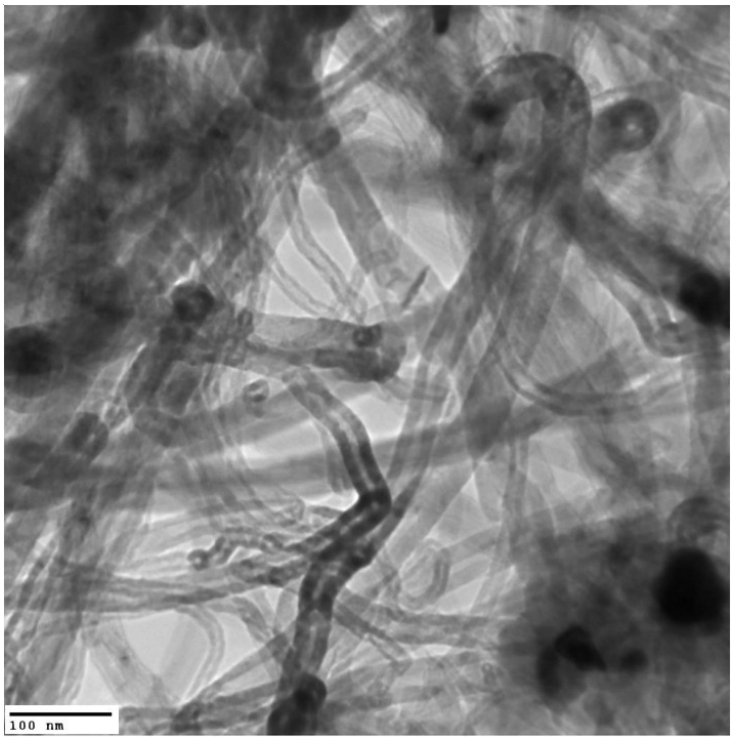

Figure 3-2: TEM micrograph of the as-received multiwalled CNT material.

The selected area diffraction pattern in Figure 3-3b indicates the aluminum matrix comprised mostly high angle grain boundaries. It has already been shown that during roll bonding of aluminum, the deformation imposed during one rolling pass with a 50% reduction is only sufficient to produce a subgrain structure, where low angle boundaries (with misorientations <15º) dominate between grains [4]. The subgrain structure remains after 2 cycles, but the dislocation density increases. Following 3 roll bonding cycles the dislocation density is dramatically reduced and grains show broad contours within them that suggest high internal stress [26]. At this stage subgrains are still dominant; however some of their boundaries are well-developed and have large misorientations. An ultrafine grained structure with primarily high angle grain boundaries becomes dominant after 4 cycles of roll bonding. This ultrafine grained microstructure is indicated by the dense and nearly continuous distribution of spots in the diffraction patterns [4], which is consistent with the selected diffraction pattern shown in Figure 3-3a. The combination of accumulative roll bonding differs from previous studies of

roll bonding alloy sheets with CNT powders, since the final structure was not repeatedly rolled a minimum of 4 passes each at 50% reduction, otherwise the final matrix structure will consist primarily of subgrains [11-12].

Due to non-uniform strain distributions which may occur during rolling [27], the distribution of high angle grain boundaries and grain thickness may vary depending on the thickness location [28-30]. Typically, larger shear strains are produced in the near surface region, and this effect is particularly enhanced when no lubrication is used during rolling [31]. As a result, the grain size is typically finer near the surface due to a higher amount of shear strain, resulting in a larger amount of accumulated dislocations and grain subdivision [30]. Clearly, the strain gradient and strain path during deformation play an important role in the formation of geometrically necessary dislocations and ultrafine grain sizes [32-34].

In the case of ARB, the shear strain localized at the surface of any individual pass is distributed during subsequent stacking or folding operations, hence the distribution of deformation eventually becomes uniform with increasing the number of cycles. However the grain size is also influenced by recrystallization and growth resulting due to an adiabatic temperature rise during rolling [30]. Consequently, although ARB is useful in achieving a more uniform structure through the thickness of the sheet, there may ultimately be a limiting grain size for a given material regardless of how many passes are imposed.

The three rings observed in diffraction pattern in Figure 3-3a are corresponding with the multiwalled CNTs. The average measured d-spacing values for the three diffraction rings observed were 3.50, 2.11, and 1.22 Å, which are within 1% of the spacing values observed for the (002), (004), and (110) Miller indices of the hexagonal unit cell suggested by Keller et al. [35] for CNTs. The first and most intense ring corresponds well with the reflections observed for the graphene spacing found in multiwalled CNTs [35], confirming that these are present in the composite. EDX analysis was conducted on Figure 3-3b revealed strong Al and C peaks for the composite material.

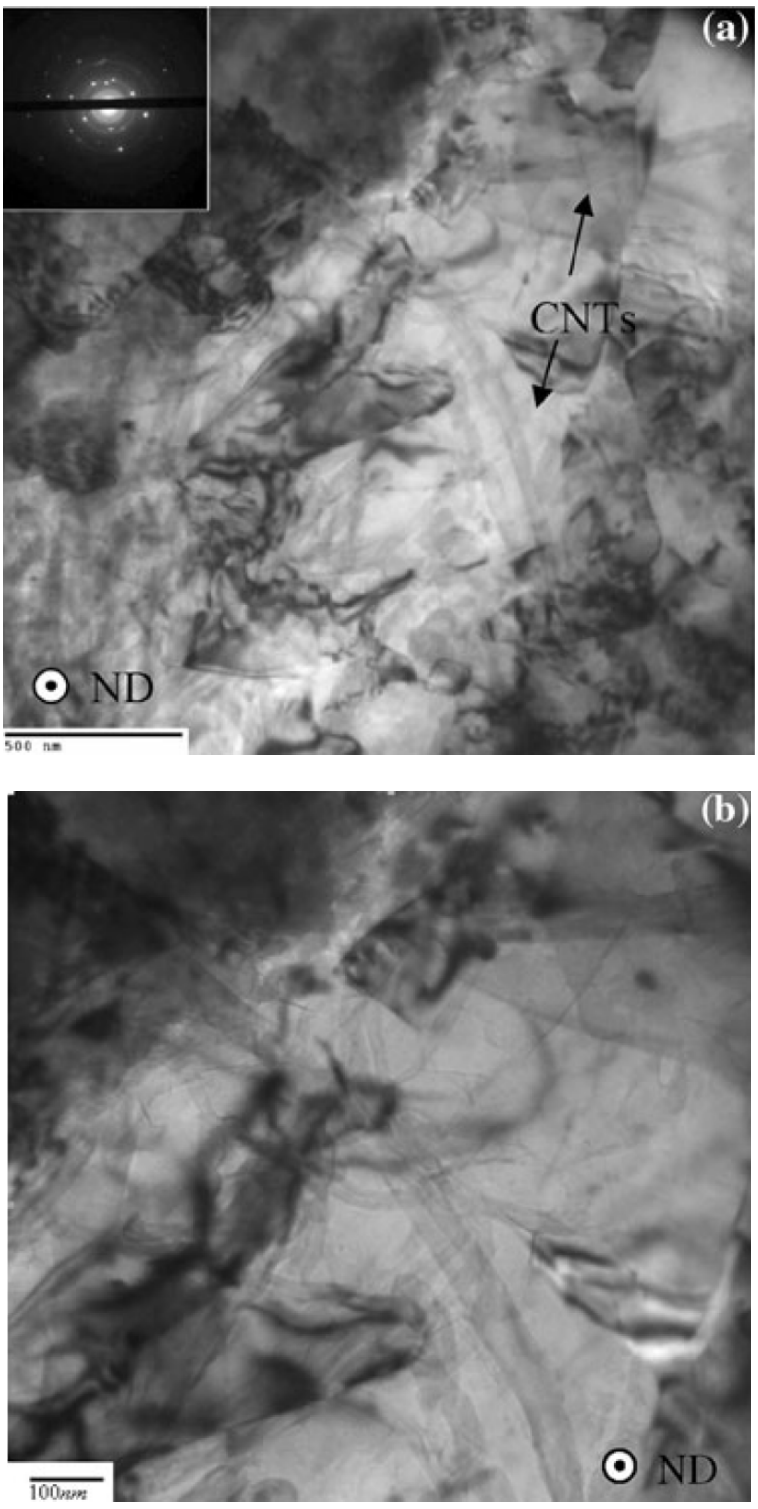

Figure 3-3: TEM micrograph of (a) the roll bonded CNT reinforced aluminum composite layer with selected area diffraction pattern when viewed along the normal direction of the sheet (ND), and (b) the individual CNTs in the matrix.

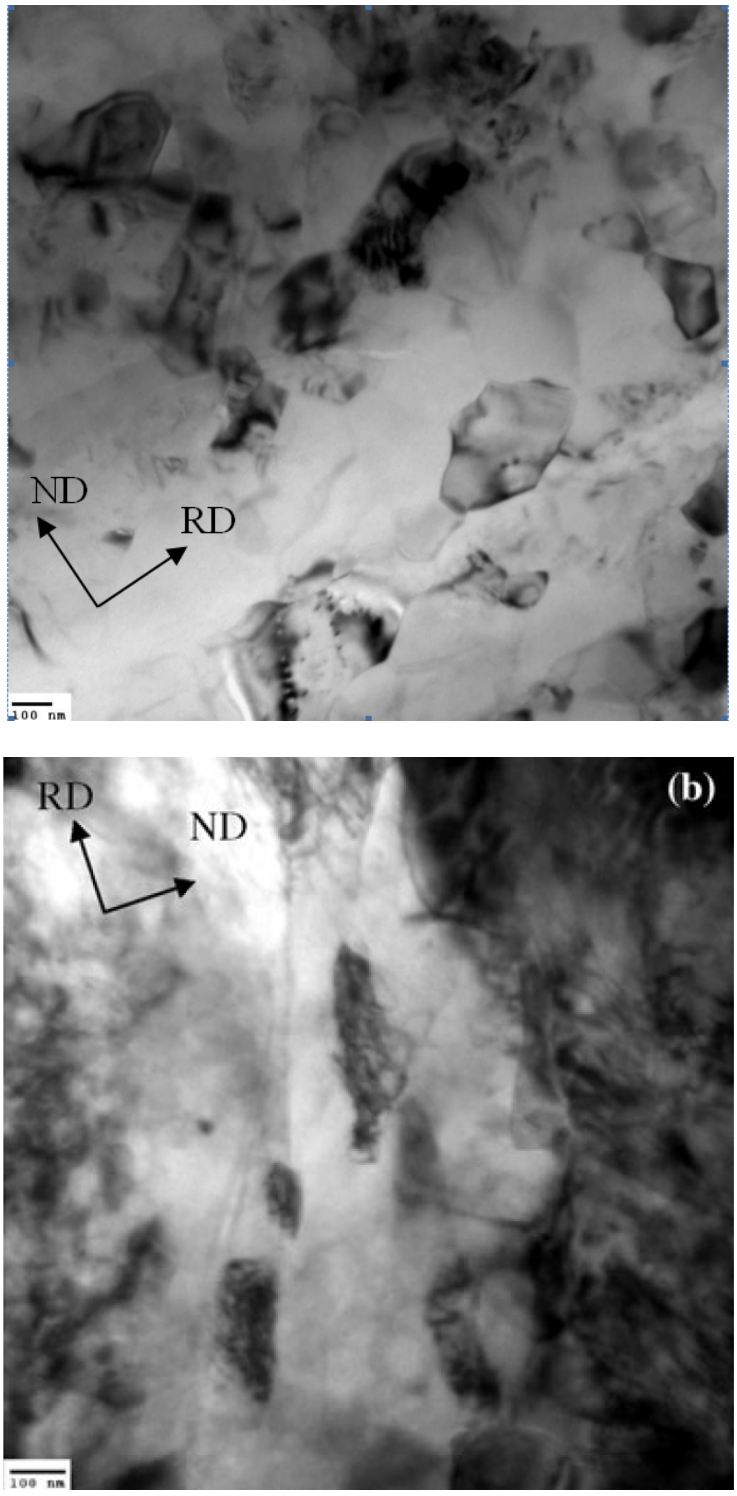

Figure 3-4: TEM micrograph of the cross section of the roll bonded CNT reinforced aluminum composite material after 4 passes.

3.3.2 CNT orientation and adhesion at the interface

The properties of CNTs are dependant on their orientation, and so this was investigated by mechanically delaminating the sheets following roll bonding, and observing the CNTs dispersed between the sheets. This was done by mechanically delaminating and peeling apart the sheets following the roll bonding operation and examining the surface using SEM, as shown in Figure 3-5. The surface revealed a non-uniform distribution of CNTs which were mostly aligned flat to the surface of the sheet. Although the CNTs were more dispersed than in the as-received material, some entangled bundles of CNTs could also be observed (see Figure 3-5b). There was also evidence of aluminum fracture surfaces created by the delamination, since metallic bonding between the aluminum sheets is promoted during roll bonding.

Since the delamination process may disrupt the CNTs from their original orientation, a cross-section was also heavily etched with HF to expose the CNTs. The sheet interfaces are revealed due to preferential etching, allowing removal of the aluminum material from the sheet interfaces and avoiding mechanical disruption their arrangement. Figure3-6a shows the CNTs at the interface, with the majority of CNTs axially aligned in the RD or TD directions. Some of the CNTs were observed to emerge from the aluminum matrix, indicating that there was intimate contact promoted between the CNTs and the aluminum (see Figure 3-6b). This suggests that adhesion has been promoted between with the surrounding matrix.

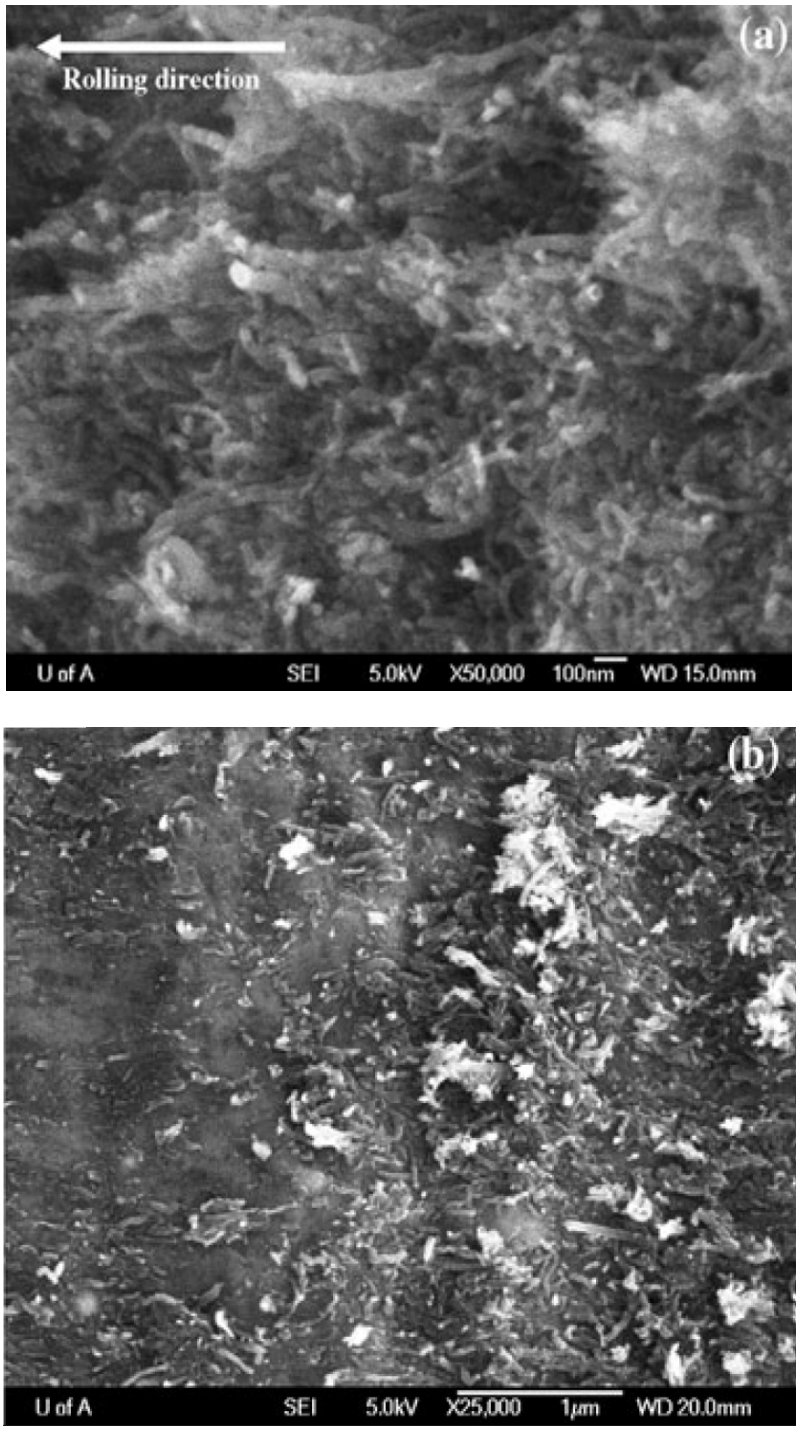

Figure 3-5: SEM image of the interface of the roll bonded composite sheets after they were mechanically delaminated.

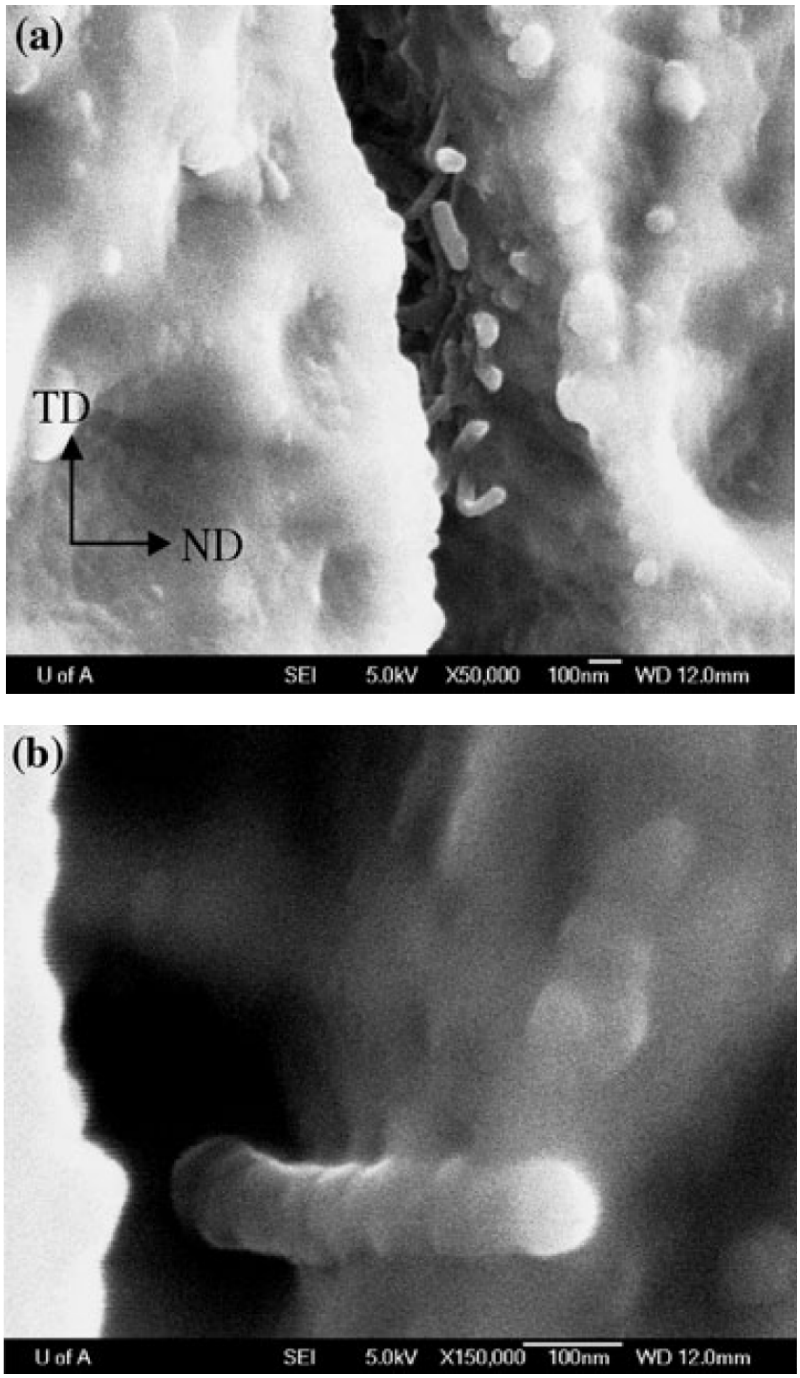

Figure 3-6: SEM image of (a) the cross section of the reinforced layer in the roll bonded CNT reinforced aluminum composite material following etching with HF, and (b) a single CNT embedded in the aluminum.

3.3.3 Rupture of CNTs during rolling

By optimizing the distribution of CNTs and uniformity of the matrix microstructures demands repetitive rolling of the sheets. A highly uniform distribution of nanotubes in the through-thickness direction provided that CNTs are only introduced once before the initial rolling cycle, and several cycles are applied. For example, since the number of reinforced layers increases exponentially during repeated processing, the number of CNT reinforced layers is equal to $(2^n\text{-}1)$, where n is the number of roll bonding cycles. Hence the resistance of the CNTs to rupture is a key feature to achieving a uniform distribution of reinforcement in the final composite.

Alternatively, another key feature of the ARB fabrication process is that it may permit the concentration of CNTs to be increased by repeatedly producing an additional reinforced layer between the stacked sheets prior to each rolling cycle. A prerequisite for the fabrication process is for the majority of nanotubes to remain intact during repeated rolling in order to achieve a satisfactory yield in the final bulk composite. To assess the integrity of the CNTs during rolling, the diameters were measured for 110 nanotubes in the as-received material, as well as for 117 nanotubes subjected to 4 rolling cycles, using TEM micrographs.

The as-received CNTs clearly exhibit a bimodal size distribution in terms of their diameters, see Figure 3-7. This may occur depending on the synthesis route taken to fabricate the multiwalled CNTs [36]. Following 4 roll bonding cycles, the CNTs with diameters approximately >30 nm appear to have been retained in the composite. Multiwalled CNTs with larger diameters may sustain larger strains when subjected to radial compression [16, 37]. In addition, the larger CNTs in the base material also tended to have a higher apparent wall thickness (see Figure 3-8a), which indicates these consisted of a greater number of walls. It has been shown using continuum mechanics that the critical buckling stress during radial loading of a multiwalled CNT will increase with the number of walls since the pressure is more evenly distributed over a greater number of walls [38]. As show in Figure 3-6, one can assume that the primary loading condition during rolling is compressive loading along the radial direction of the

CNTs. Consequently, it is not surprising that the population of CNTs which survived most readily are those which have greater wall numbers, corresponding with those that also had outer diameters >30 nm, see Figure 3-8b.

However, one other property of multiwalled CNTs is that the radial buckling stress of the CNTs should increase as the inner diameter decreases [38]. In contrast the CNTs which had a smaller inner radius did not survive the loading cycles during rolling in the present work. It is possible that this may be accounted for by the biaxial loading conditions imposed during rolling. Due to the mismatch in the yield strength and stiffness of carbon nanotubes versus aluminum, CNTs are exposed to high axial tensile stresses during the rolling process. Hui-Shen et al. [39] have shown that under combined axial and radial loading multiwalled CNTs will buckle sooner than when only radial force is applied. Therefore, the axial tensile stress which contributes to buckling is lower in CNTs with a larger diameter since these have a higher number of walls and there is a greater effective cross-sectional area. Under the same loading conditions during rolling, there will be more pressure on CNTs having smaller diameter. The buckling process is a precursor to rupture of the CNTs since the formation of kinks and defects occurs during buckling [40], ultimately leading to failure. Hence the CNTs which have prematurely buckled are not likely to survive the rolling process.

Evidence of ruptured CNTs could be found using by TEM and EDX analysis. The chemical composition was measured at the 3 points showing in Figure 3-9 and the results are given in Table 3-1. A progressively decreasing fraction of carbon could be detected at points further from the end of the broken CNT. This indicates the presence of carbon in locations of the aluminum matrix devoid of CNTs. In previous studies it has been shown that the results of these ruptures would be formation of highly defected carbon structures such as graphite layers [41], these may dissociate into the aluminum matrix and form a solid solution with carbon contents similar to that observed in point C in Figure 3-9. It is suggested that this carbon was contributed primarily by the CNTs with diameters <30 nm that ruptured during rolling.

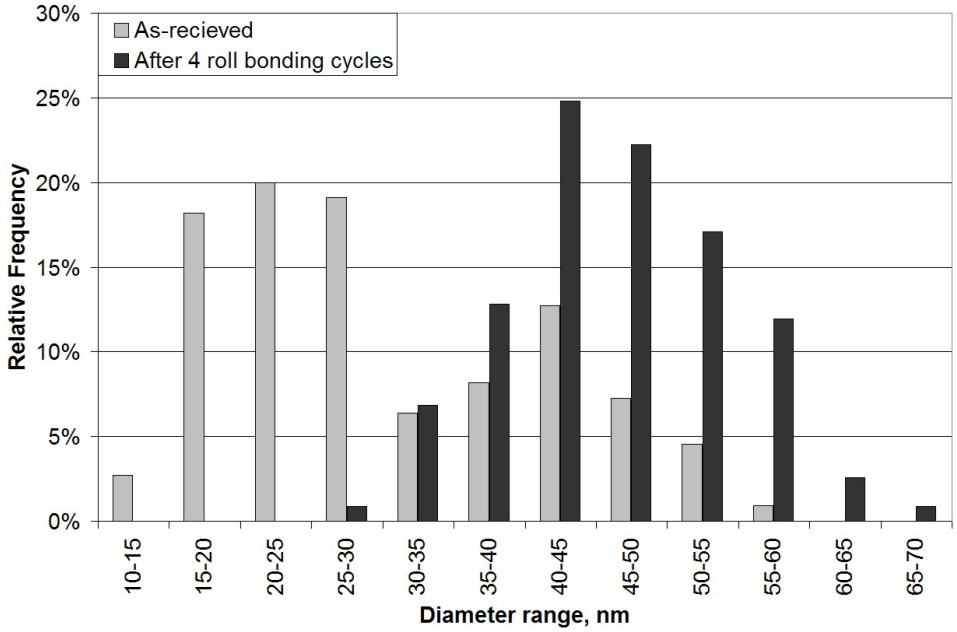

Figure 3-7: Distribution of carbon nanotube diameters in the as-received material, and roll bonded aluminum metal matrix composite. The number of samples measured was 110 and 117 for the as-received and roll bonded CNT populations respectively.

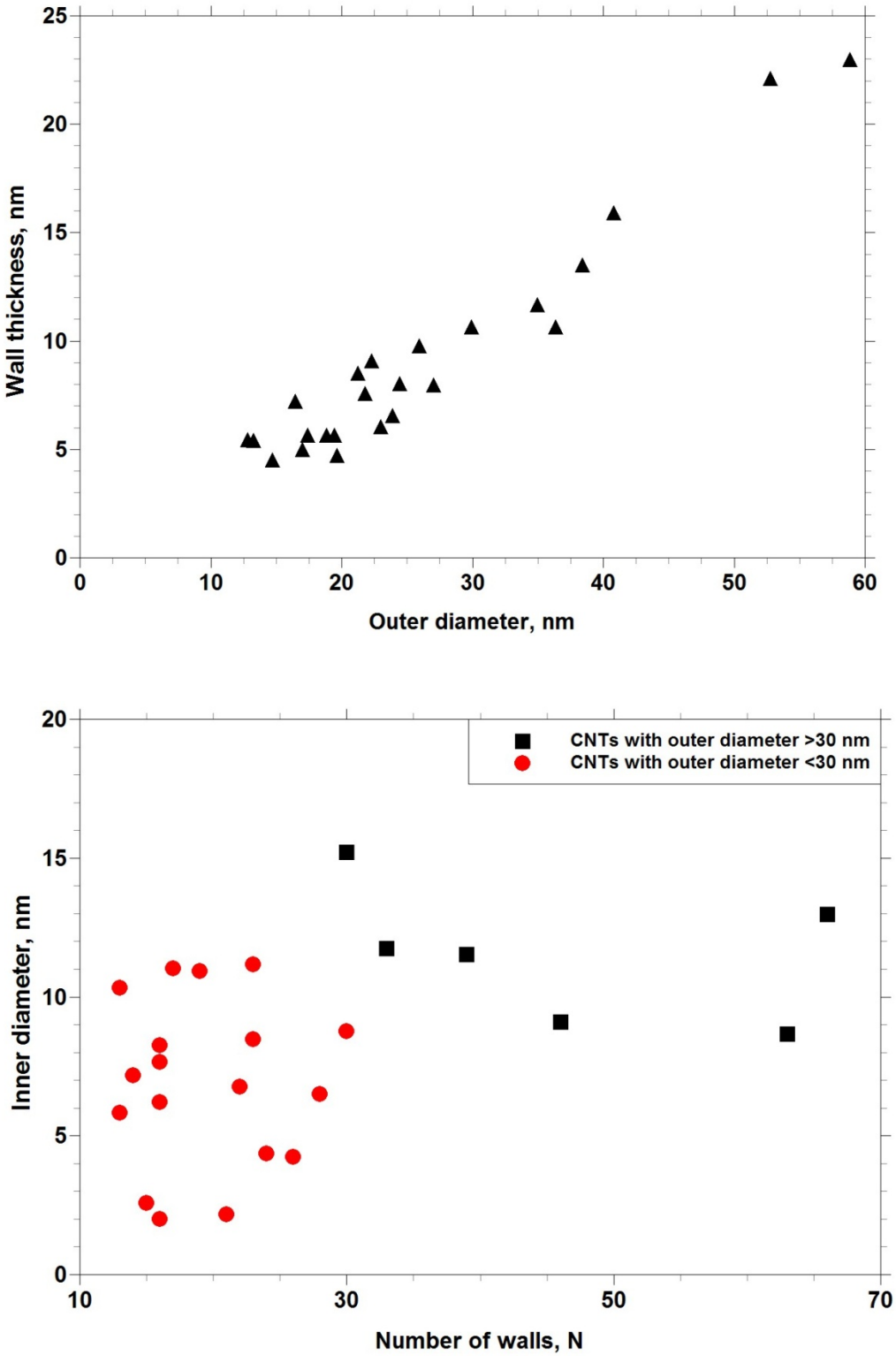

Figure 3-8: (a) Diameter and wall thickness measurements for the CNT base material, and (b) number of walls versus inner diameter for CNT base material.

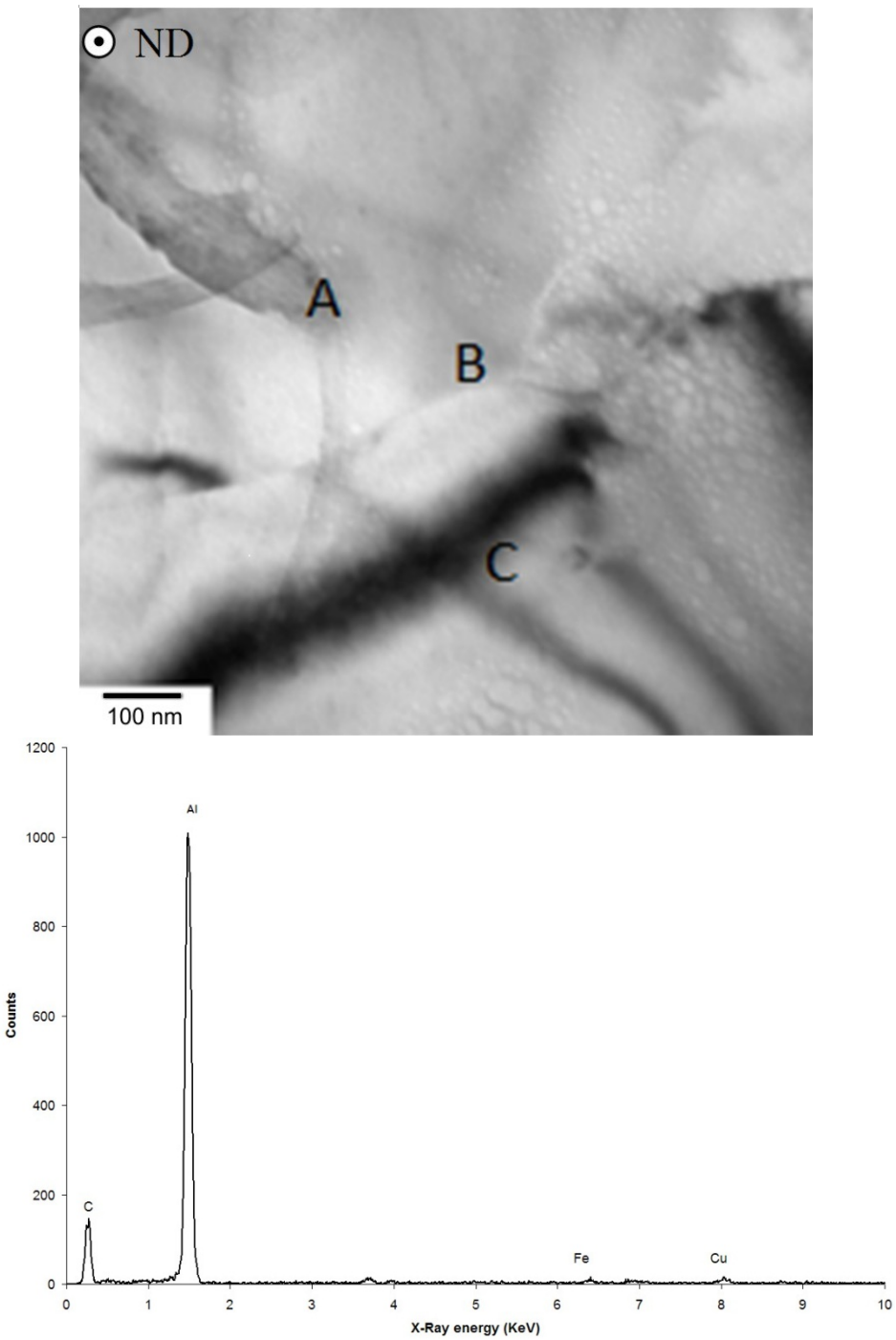

Figure 3-9: (a) TEM micrograph of the roll bonded composite with the end of a broken CNT at A, and (b) EDX spectrum of the sample at point A.

Table 3-1: EDX quantification in at% measured at points A, B and C of Figure 3-9.

Point	Al	C	Si	Fe	Cu	Ca
A	68.0	30.82	0	0.4	0.77	-
B	76.71	18.05	0	0.06	0.79	4.41
C	94.4	2.21	0.02	0.59	0.87	1.92

3.4 Conclusion

In conclusion, it has been shown that a modification of the accumulative roll bonding may be used to disperse CNTs into an aluminum alloy. The process was effective in producing a composite microstructure with multi-walled CNTs embedded in an ultrafine grained aluminum matrix. The CNTs with diameters >30 nm and more than 30 walls readily endured 4 consecutive roll bonding operations, and their multi-walled structure was preserved in the final composite.

3.5 Bibliography

[1] Y. Saito, H. Utsunomiya, N. Tsuji, T. Sakai, Acta Mater 47 (1999) 579-583.

[2] L.R. Vaidyanath, M.G. Nicholas, D.R. Milner, British Welding Journal 6 (1959) 13–28.

[3] N. Tsuji, Y. Saito, S.H. Lee, Y. Minamino, Adv Eng Mater 5 (2003) 338-344.

[4] Y. Saito, N. Tsuji, H. Utsunomiya, T. Sakai, R.G. Hong, Scripta Mater 39 (1998) 1221-1227.

[5] N. Tsuji, Y. Saito, H. Utsunomiya, S. Tanigawa, Scripta Mater 40 (1999) 795-800.

[6] P.J. Hsieh, Y.C. Lo, J.C. Huang, S.P. Ju, Intermetallics 14 (2006) 924-930.

[7] G.H. Min, J.M. Lee, S.B. Kang, H.W. Kim, Mater Lett 60 (2006) 3255- 3259.

[8] G.P. Dinda, H. Rosner, G. Wilde, Scripta Mater 52 (2005) 577-582.

[9] K. Mizuuchi, K. Inoue, K. Yamauchi, K. Enami, M. Itami, Y. Okanda, Mat Sci Eng a-Struct 316 (2001) 93-101.

[10] C. Lu, K. Tieu, D. Wexler, J Mater Process Tech 209 (2009) 4830-4834.

[11] Y.H. Li, W. Housten, Y.M. Zhao, Y.Q. Zhu, Nanotechnology 18 (2007) -.

[12] D. Lahiri, S.R. Bakshi, A.K. Keshri, Y. Liu, A. Agarwal, Mat Sci Eng a-Struct 523 (2009) 263-270.

[13] S. Iijima, C. Brabec, A. Maiti, J. Bernholc, J Chem Phys 104 (1996) 2089-2092.

[14] M.R. Falvo, G.J. Clary, R.M. Taylor, V. Chi, F.P. Brooks, S. Washburn, R. Superfine, Nature 389 (1997) 582-584.

[15] S. Iijima, Nature 354 (1991) 56-58.

[16] M.M.J. Treacy, T.W. Ebbesen, J.M. Gibson, Nature 381 (1996) 678-680.

[17] R.S. Ruoff, D.C. Lorents, Carbon 33 (1995) 925-930.

[18] P. Quang, Y.G. Jeong, S.C. Yoon, S.H. Hong, H.S. Kim, J Mater Process Tech 187 (2007) 318-320.

[19] W. Salas, N.G. Alba-Baena, L.E. Murr, Metall Mater Trans A 38A (2007) 2928-2935.

[20] K. Morsi, A. Esawi, J Mater Sci 42 (2007) 4954-4959.

[21] T. Kuzumaki, K. Miyazawa, H. Ichinose, K. Ito, J Mater Res 13 (1998) 2445-2449.

[22] R. Zhong, H.T. Cong, P.X. Hou, Carbon 41 (2003) 848-851.

[23] T. Noguchi, A. Magario, S. Fukazawa, S. Shimizu, J. Beppu, M. Seki, Mater Trans 45 (2004) 602-604.

[24] A.M.K. Esawi, M.A. El Borady, Compos Sci Technol 68 (2008) 486-492.

[25] L.J. Ci, Z.Y. Ryu, N.Y. Jin-Phillipp, M. Ruhle, Acta Mater 54 (2006) 5367-5375.

[26] R.Z. Valiev, F. Chmelik, F. Bordeaux, G. Kapelski, B. Baudelet, Scripta Metall Mater 27 (1992) 855-860.

[27] N. Kamikawa, N. Tsuji, X.X. Huang, N. Hansen, Acta Mater 54 (2006) 3055-3066.

[28] N. Tsuji, Y. Saito, Y. Ito, H. Utsunomiya, T. Sakai, Ultra-fine grained ferrous and aluminum alloys produced by Accumulative Roll Bonding, in, Ultrafine Grained Materials TMS, Nashville, TN, USA, 2000, pp. 207-218.

[29] Y. Ito, N. Tsuji, Y. Saito, H. Utsunomiya, T. Sakai, J Jpn I Met 64 (2000) 429-437.

[30] S.H. Lee, Y. Saito, N. Tsuji, H. Utsunomiya, T. Sakai, Scripta Mater 46 (2002) 281-285.

[31] N. Kamikawa, T. Sakai, N. Tsuji, Acta Mater 55 (2007) 5873-5888.

[32] N. Tsuji, R. Ueji, Y. Ito, Y. Saito, Recrystallization—Fundamental aspects and relations to deformation microstructure, in, Proceedings of the 21st RISØ International Symposium on Material Science, RISØ National Laboratory, Denmark, 2000, pp. 607.

[33] M.F. Ashby, Philos Mag 21 (1970) 399.

[34] Y. Iwahashi, Z. Horita, M. Nemoto, T.G. Langdon, Acta Mater 46 (1998) 3317-3331.

[35] T.M. Keller, M. Laskoski, M. Osofsky, S.B. Qadri, Physica Status Solidi a-Applications and Materials Science 205 (2008) 1585-1591.

[36] I. Willems, Z. Konya, J.F. Colomer, G. Van Tendeloo, N. Nagaraju, A. Fonseca, J.B. Nagy, Chem Phys Lett 317 (2000) 71-76.

[37] T. Hertel, R.E. Walkup, P. Avouris, Phys Rev B 58 (1998) 13870-13873.

[38] C.Y. Wang, A. Mioduchowski, J Appl Phys 101 (2007) -.

[39] H.S. Shen, C.L. Zhang, Int J Solids Struct 44 (2007) 1461-1487.

[40] C.P. Deck, J. Flowers, G.S.B. McKee, K. Vecchio, J Appl Phys 101 (2007)

[41] D.S. Tang, L.C. Chen, L.J. Wang, L.F. Sun, Z.Q. Liu, G. Wang, W.Y. Zhou, S.S. Xie, J Mater Res 15 (2000) 560-563.

4 Experimental investigation of mechanical damping of carbon nanotube reinforced aluminum composites fabricated by ARB

4.1 Introduction

A key feature of nanostructured metals is strengthening by structural refinement. In recent years, ultrafine grained materials produced by severe plastic deformation (SPD) with grain sizes less than 1 μm have drawn much attention. Structure refinement may be obtained by processes such as accumulative roll bonding (ARB) [1], equal channel angular extrusion (ECAE) [2], and high pressure torsion (HPT) [3]. It is of interest to relate the strength properties of the processed materials to microstructure characteristics based on different models for various strengthening mechanisms. The microstructural characteristics that develop during fabrication of nanostructures by deformation include the structural morphology, grain boundary spacing, grain boundary misorientation and the dislocation density [4].

These microstructural characteristics are affected by the deformation process parameters, such as strain, strain rate, and deformation temperature. In addition, the material parameters such as stacking fault energy and impurities also affect the microstructure characteristics. Materials produced through deformation may have nanocrystalline grains with elongated or equiaxed appearance. The elongated structure is often observed in nanostructures produced by monotonic deformation, such as cold rolling [5] and ARB [1]. An equiaxed structure is mostly observed in complex deformation processes, such as multi-direction forging [6], and surface mechanical attrition [7]. ARB processed alloys, are comprised of ultra-fine grains [8,9], which are separated by high angle grain boundaries (with misorientations larger than 15º) [9].

The mean grain boundary misorientation increases, with increasing strain. This is due to the increase of the fraction of high angle grain boundaries that are formed during the transformation of low angle dislocation boundaries to high angle dislocation boundaries by the accumulation of dislocations [9,10]. Since

both deformed and recrystallized grains exist, the measured grain boundary misorientation angles in the deformed nanostructures exhibit a bimodal distribution, with one peak at lower angles and another at higher angles [12].

Materials produced through deformation have both individual dislocations and dislocation tangles between the grain boundaries. The dislocation density varies from grain to grain, however, and is highly dependent on the material and the deformation conditions. For example, in a pure aluminum sample that is significantly deformed, enhanced recovery occurs after severe plastic deformation, and recovery is essentially complete immediately after the deformation is complete [4,13]. This results in low dislocation density in aluminum grains after deformation.

The Vickers microhardness values of accumulative roll bonded commercially pure aluminum are shown in Fig 4-1. An immediate increase in microhardness (by a factor of 2) occurs even after the first cycle. The increase in hardness values after subsequent cycles is small in comparison to the first cycle. The observed increase after the first pass is due to the increase in dislocation density and the interaction between them (strain hardening) [11]. At higher strain values the hardness value reaches a saturation point [14, 15], since the dislocation generation during plastic deformation reaches a balance with dislocation annihilation in the dynamic recovery process and a steady-state dislocation density is achieved [11].

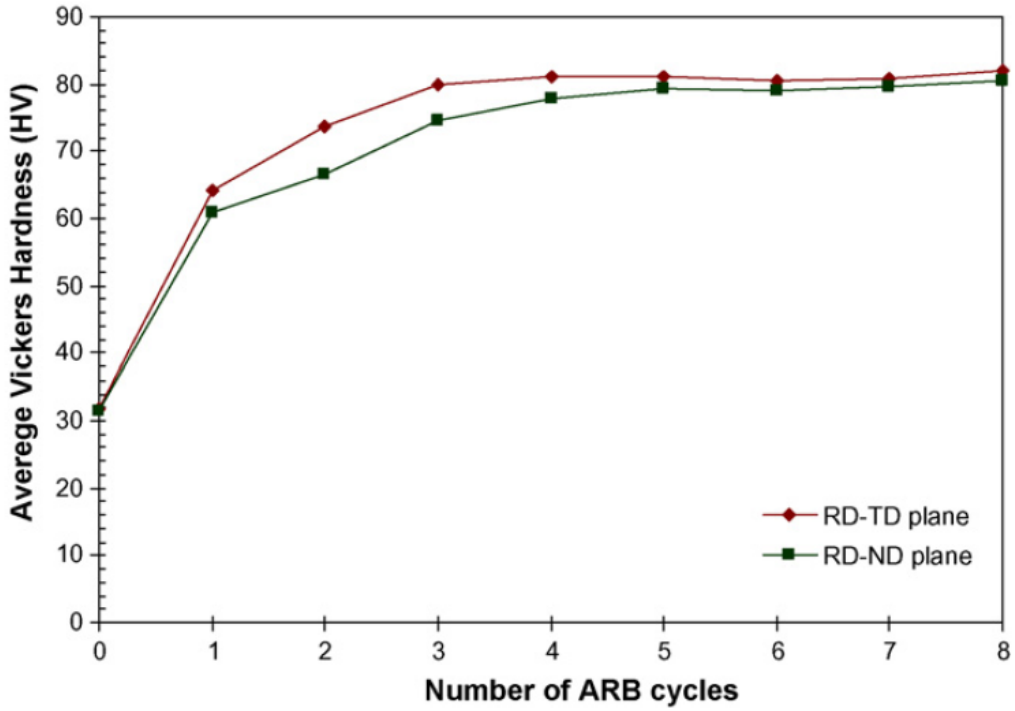

Figure 4-1: Variation of Vickers microharness with respect to accumulative strain in ARB samples [11].

4.1.1 Correlation between structural parameters and mechanical properties

The tensile properties of many nanostructured metals and alloys have been studied. Some of the common properties observed include:

- Very high strength, several times higher than coarse grained samples.
- Limited strain hardening and small uniform elongation (before ultimate tensile strength point).
- Relatively large overall elongation (before failure).

The strengthening in ARB-processed commercially pure aluminum may be attributed to strain hardening (σ_ρ) and grain refinement hardening (medium to high angle grain boundaries) σ_{gb}.

$$\sigma = \sigma_0 + \sigma_\rho + \sigma_{gb} \qquad \text{(Equation 4-1)}$$

where σ_0 is the internal stress, σ_ρ is calculated on the assumption of dislocation hardening, therefore, proportional to $\rho^{1/2}$ [11]. The contribution of σ_{gb} is based on

the Hall-Petch strengthening mechanism, where strength varies inversely with the square root of average grain diameter [4, 16].

Research has shown that, strain hardening plays an important role in increasing the strength and the formation of dislocation cells in order to increase the strength in the first 3 cycles. After 4 cycles, the increase in strength is mainly due to the formation of ultrafine grains and strain hardening has less effect [11].

Haung et al. [4] observed an unusual mechanical behavior in aluminum during low temperature annealing at 150ºC for 30 minutes (see curve 2 in Figure 4-2), which is observed to cause the yield strength to increase. When the same sample is deformed after annealing, the yield strength decreases (curve 3 in Figure 4-2), and the major microstructural changes were reported to be a decrease in dislocation density after annealing and reintroducing them in the sample by cold rolling. It was argued that after dislocations have been removed by the processes of climb and annihilation during annealing, tensile stresses above the yield point are needed to activate the dislocation sources in the grains of the material. When the dislocations are reintroduced, yield stress will therefore decrease because dislocation sources have now been reformed.

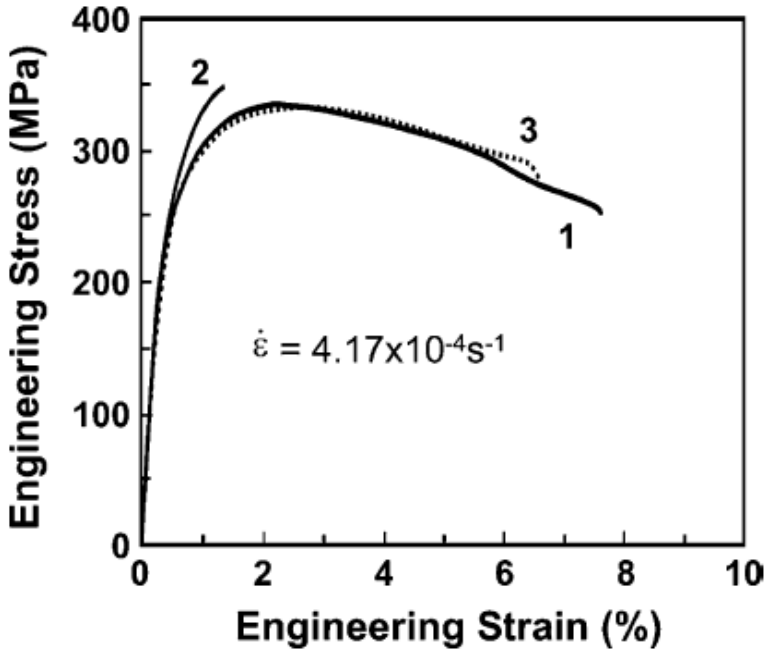

Figure 4-2: Tensile stress-strain curves for nanostructured aluminum. As processes by six cycle ARB to an equivalent strain of 4.8. (curve 1); same material as 1 plus annealing at 150ºC for 30 min (curve 2); same as 2 but deformed 15% by cold rolling (curve 3) [4].

This indicates that the presence of a certain amount of dislocations in the nanostructured tensile specimen may be a softening mechanism rather than a strengthening mechanism. Consequently, the availability of dislocation sources and the lack of them may notably influence the yield stress.

4.1.2 Elastic modulus of Nanocrystalline Metals

Most experimental studies of the mechanical behavior of the ultrafine grain materials are mostly focused on the dependence of strength on grain size, and to a lesser extent, the elastic behavior of the material. There are conflicting results about the Young's modulus (E) with grain size; most experimental results indicate a reduction in Young's modulus with grain size [17, 18]. Fougere et al. [17] found a decrease in Young's modulus of nanocrystalline Fe with increasing porosity. Chen et al. [19] explained that since E is a measure of the bonding between the atoms, the decrease in E in nanocrystalline materials may be explained by the increase of volume fraction of grain boundary atoms. Sanders et al. [18] and Krstic et al. [20], attributed the reduction of E to porosity and assumed the E of material is independent of grain size. On the other hand some some research studies show almost no effect with change in grain size. Porosity and stress concentration associated with pores has a significant effect in Young's modulus of nanocrystalline materials [20]. The reduction in E is governed by the number of pores per unit volume, and therefore, variation of Young's modulus is directly related to the level of porosity in the material. The results of different studies imply that porosity is an important factor in decreasing the Young's modulus value.

Kim et al. [21] isolated both effects and examined them to rationalize the experimental data. They explained that when the grain size is smaller than about 100nm the volume fraction of the boundary phases becomes important, and the volume fraction of the crystalline decreases rapidly with decreasing grain size. The elastic modulus at a constant porosity level decreased very slowly at grain size greater than 20nm, the decrease is grain size was much faster at grain size lower than 20nm. This trend was the same, independent of the amount of porosity.

On the other hand, the effect of porosity was much larger than grain size, meaning since these is nanocrystalline materials, usually contain some porosity, the decrease of elastic modulus value the contribution of the grain size may be ignored for nanocrystalline materials.

4.2 Experimental methods

4.2.1 Preparation of the composite

CNTs with 10-70 nm diameter and 5-10 μm length with purity greater than 95% were used in this research. Commercially pure aluminum strips of 1 mm thickness and 99.5% purity were used as the matrix of the material.

The multiwall CNTs were ultrasonically agitated in 2-propanol solution for 30 minutes and then heated in order to evaporate the alcohol and obtain a highly concentrated suspension of CNTs. After degreasing the aluminum and wire brushing the surfaces, the sheets were coated once using a spatula, only at the initial cycle, with the concentrated CNT suspension and allowed to dry. The sheets were then stacked together making a 2 mm thick sandwich that was accumulatively roll bonded 5 times at room temperature with intermediate degreasing and wire brushing. Each sample was accumulatively roll bonded with 75% reduction in thickness; all the rolling passes were performed along the same direction and each cycle was followed by annealing at 673 K for 1.5 hours. The final thicknesses of all 6 samples were between 121μm to 250 μm.

The content of the CNT in the composites was determined by weighting the as-received aluminum foil before and after applying CNT on them. The elastic modulus and the internal friction of the roll bonded composites produced with the average CNT contents shown in Table 4-1 were compared with a bulk aluminum sample with same thickness.

Table 4-1: Weight percent CNT and the initial surface density of the samples.

Amount of CNT (wt%)	Surface Density (µg/mm2)
0.050	0.700
0.100	1.300
0.170	3.000
0.238	7.500
0.500	13.200

4.2.2 Microstructural characterization

Composite strips were first cross sectioned perpendicular to rolling direction, then mounted in epoxy resin and polished to observe their microstructure by optical microscopy. Transmission electron images of CNT reinforced composite foils were obtained using a JEOL 2010 microscope, operated at 200keV. The distribution of the CNTs on the delaminated surface of the composite foils was observed by scanning electron microscope JEOL 6301F operated at 5kV.

4.2.3 Evaluation of mechanical properties

The modulus of elasticity of all the composite foils was evaluated through a cantilever beam test. The dimensions of the beam specimen were 60 mm by 15 mm and the thickness of the material was 0.15-0.25 mm. In this method, the test specimen is loaded as a simple cantilever beam. One end of the beam is supported and the free end is progressively deflected. This procedure involves measurement of the applied force and the corresponding deflection displacement of the cantilever beam. The testing fixture is shown in Figure 4-3. This test fixture consists of a specimen holder, a microscale to measure the force on the beam in grams, and digital dial gauge that measures the deflection to within 0.001 mm. The specimen is firmly clamped with its long side parallel to the gripping plate. The dial gauge is fixed at zero deflection at the point on the sample where the

loading pin just touches the beam. As the loading pin is moved upward, it forces the specimen to bend. When a maximum deflection of a few millimeters is reached, the position and force on the beam is recorded during the unloading of the beam in several increments in order to ensure that no plastic component is included in the measurement.

Figure 4-3: Cantilever beam test setup.

During the unloading of the specimen, the force F decreases, as the beam curvature or deflection decays. Assuming that the beam has a constant cross section, with uniform properties and a large beam length to depth ratio, the deflection of the loaded end of a cantilever beam in the purely elastic range is calculated as follows:

$$\delta = \frac{Fl^3}{CEI} \qquad \text{(Equation 4-2)}$$

where C equals 3 for rectangular cross sections, E is Young's modulus (N/m^2), L is the length of the sample (m), F is the force (N), b is the width of the sample (m), h is the thickness of the sample (m), δ is the amount of deflection of the beam (m), and I is the moment of inertia as defined in Equation 4-3.

$$I = \frac{bh^3}{12} \qquad \text{(Equation 4-3)}$$

To verify the results obtained from the bending test, the elastic modulus and the internal friction of the composite specimens were also measured by impulse excitation of vibration method [22]. This method measures the fundamental resonant frequency of the specimen by mechanically exciting it with a singular elastic strike from an impulse tool (hammer), and the resulting mechanical vibrations of the specimen are transformed into electric signals by a transducer. The signals are analyzed and the resonant frequency is measured. The first natural frequency, the dimensions, and the mass of the specimen are then used to calculate the Young's modulus (Equation 4-4). The test setup is shown in Figure 4-4. This figure consists of an impulse and suitable pick up transducer to convert the mechanical vibrations to electrical signals, an electric system, and a support system.

As mentioned above, the Young's modulus for a rectangular bar is calculated by the equation 4-4:

$$E = 0.9465\left(\frac{mf^2}{b}\right)\left(\frac{L^3}{h^3}\right)T_1 \qquad \text{(Equation 4-4)}$$

where f is the fundamental resonant frequency (Hz), m the mass of the bar (g), T is a correction factor that is proportional to Poisson's ratio.

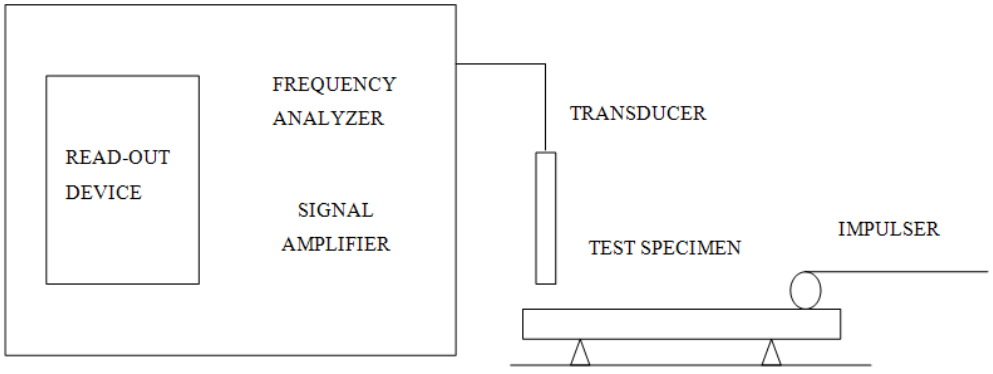

Figure 4-4: Schematic representation of a typical test apparatus for the impulse excitation of vibration method.

4.2.4 Damping behavior of reinforced Al alloy metal matrix composites

Materials with high damping capabilities, i.e. materials with high internal friction, are referred to as materials that have a high ability to dissipate mechanical vibration energy [23]. These materials are valuable in applications that require noise control and suppression of mechanical vibration and wave propagation. Such applications require low-density materials and good mechanical properties that exhibit high damping capacity. This was a motivation for investigators to develop materials possessing high damping capacity, high stiffness, and low density [24]. Since these properties are dependent on microstructure characteristics, they are usually incompatible [25]. These properties can only be compatible if the microscopic mechanisms that are responsible for dissipation of vibration energy and hardening are independent of each other, by developing a two-phase composite in which each phase plays a separate role [25]. Since aluminum alloys possess low density and at the same time have high stiffness, they are the first candidates to serve as the base of these composites [24]. However, these alloys are essentially considered low damping materials and therefore have limited application in a dynamic environment. In order to increase their damping capacity, researchers have tried to improve their performance through the use of metal matrix composite (MMC) technology [24, 25].

MMCs are suitable for this goal because their processing makes it possible to modify the damping properties by selecting a high damping reinforcement second phase. Also, during the manufacturing process of MMCs, the microstructure of the metal or alloy is modified, which also modifies the mechanical property of the composite and can also be a source of energy dissipation [25].

The damping behavior of metal matrix composites may be due to a number of reasons listed below:

- *Thermal mismatch dislocation damping*: dislocation density increases due to thermal mismatch between the reinforcement and the matrix, which is an important energy dissipation source.
- *Interface damping*: sliding of the interface between the reinforcing second phase and the matrix dissipates energy.
- *The rule of mixture damping*: the nature of damping of the matrix and the reinforcing second phase may be different. This therefore leads to a rule of mixtures effect on the overall damping behavior.

4.2.5 Measurements of damping

Material damping is defined based on the decay of vibration amplitude in the material [24]. Specific damping capacity is defined by:

$$\psi = \frac{\Delta w}{w} \qquad \text{(Equation 4-5)}$$

where Δw is the energy dissipated during one cycle, w is the maximum stored energy during that cycle. Quality factor or internal friction is related to specific damping capacity by:

$$Q^{-1} = \frac{\psi}{2\pi} \qquad \text{(Equation 4-6)}$$

The damping of MMCs is directly related to each of the damping mechanisms that will be explained later in this section. The overall damping is expressed as a summation of these mechanisms, such as dislocation damping, grain boundary damping (related to the metal matrix) and reinforcing second phase versus matrix interface damping. At higher temperatures, grain boundary sliding and interface sliding are the dominating mechanism of energy absorption. On the other hand, at lower temperatures, the dominating damping mechanisms are intrinsic damping of the reinforcing particle, matrix dislocation damping and the damping at interface of the matrix and particle.

4.2.6 Damping Mechanisms

Grain boundary damping

In polycrystalline metals, grain boundaries exist that display viscous like properties. The viscous flow at grain boundaries will convert the produced mechanical energy into thermal energy as a result of internal friction at grain boundaries. The thermal energy will then be dissipated by the conductivity of the metal and heat exchange with the surroundings. The energy absorbed at grain boundaries is dependent on the magnitude of shear stress and the grain boundary per unit volume (grain size). Consequently, polycrystalline materials typically exhibits higher damping than a single crystal material. Furthermore, nanocrystaline materials would have even higher damping than coarse grained materials [23, 24].

Thermal mismatch and dislocation damping

The increase of the overall MMC damping may also be related to the increase in dislocation density in the metallic matrix as a result of thermal mismatch strain between the reinforcing second phase and metal matrix [24, 26]. These dislocations are generated to accommodate the residual thermal mismatch strains associated with the difference between the coefficient of thermal expansions of the matrix and the reinforcements. These dislocations are primarily located near the reinforcement-matrix interface and the dislocation density decreases with increasing distance from the interface.

Loss of energy occurs due to dislocations breaking away from weak pinning points (such as precipitates) under cyclic loading. This break away and sweeping motion dissipates energy in proportion to the area traversed. Accordingly, the internal friction of a material is also proportional to the dislocation density present.

To get a better perspective of internal friction caused by dislocation pinning effect, Figure 4-5 illustrates the model of dislocation motion in ultrafine grains. The grain boundaries are shown by the thick lines, the solid line shows a dislocation at high strain amplitude and the thin line shows the dislocations at

medium strain amplitude. The broken line indicates the neutral position of the dislocation. The pinning points of the dislocations are shown in the figure by big crosses for the tight pinning points at the grain boundary and small dark circles are soft pinning points (such as precipitates) [26].

At low strain amplitudes, the dislocation can only vibrate in small areas between the pinning points; therefore, the internal friction is only caused by the work associated with dislocation slip on the slip plane. At higher strains, the dislocations can move past some of the soft pinning points, so the internal friction is not only caused by the dislocation slip on the slip plane but also the unpinning mechanisms. Therefore, internal friction increases by increasing the strain amplitude because at higher strains, dislocations may break free from soft pinning points and move in a wider area. If the strain amplitude is high enough for the dislocations to escape from all the soft pinning points, the internal friction value does not depend on strain amplitude.

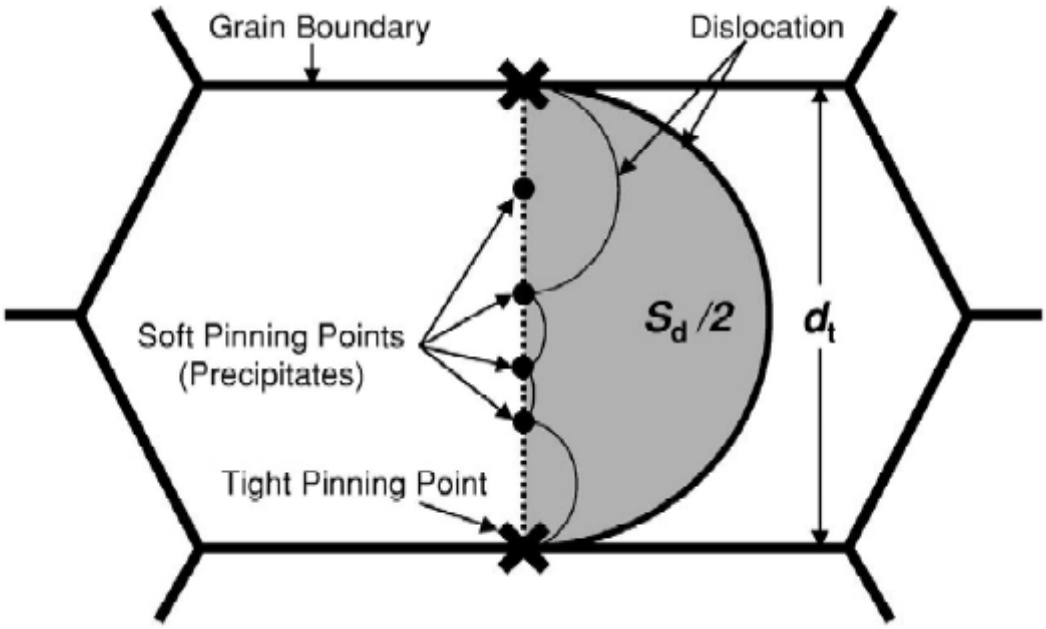

Figure 4-5: schematic illustration showing the model of dislocation motion in an ultrafine grain [26].

Interface damping

Interfaces are where the crystal structure of the metal matrix is distorted; therefore, they may affect the damping behavior of the composite. The effects of second phase/matrix interface include slip at weakly bonded interfaces and increase in dislocation density in the matrix region near the interface due to the CTE mismatch [24].

4.3 Results

4.3.1 Microstructure

Figure 4-6 shows the cross section of Al-0.23wt% CNT composite foil, after 5 cycles of ARB. The interfaces between multiple layers of aluminum are hardly visible; this indicates the effectiveness of roll bonding on promoting bonding at the interface.

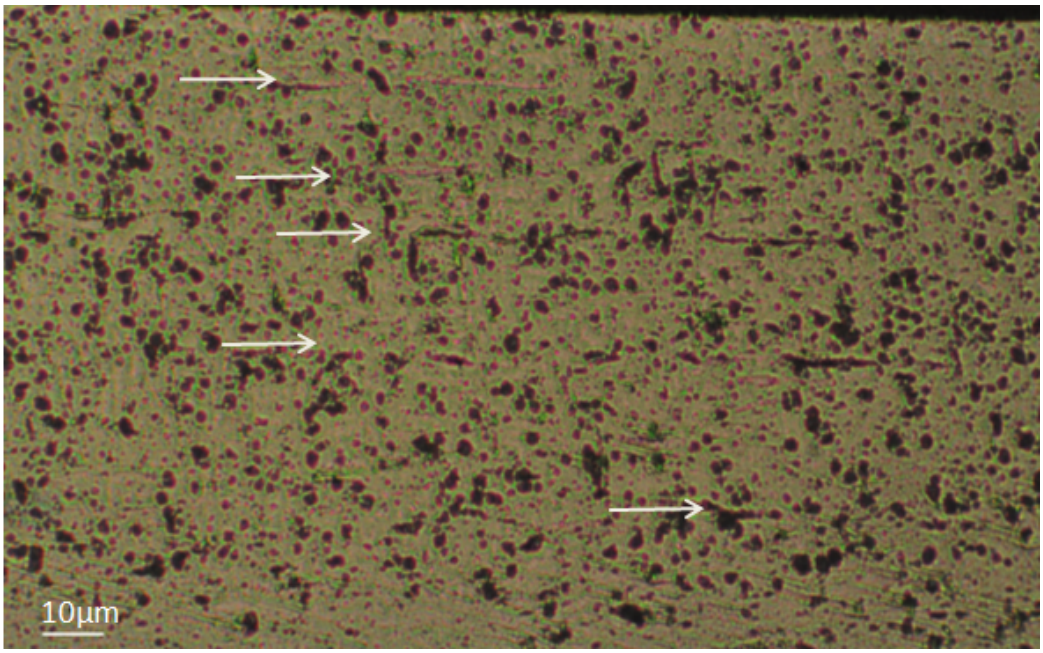

Figure 4-6: Optical micrograph of composite cross section showing roll bonded interface.

Dispersion of CNTs between the aluminum foils in the composite, was investigated by manually delaminating the roll bonded layers using a sharp blade and the deboned layer was observed using SEM. Figure 4-7 and 4-8 present the SEM images of the delaminated surface of and Al-2.3wt% CNT and Al-0.1wt%

CNT. The delaminated surface reveals the dispersed CNTs on the aluminum surface; and the sample with higher CNT content contains large bundles of CNTs. It is clear that the CNTs tend to agglomerate due to high surface tension and at high concentrations, and the roll bonding method is not effective enough to disperse and aligning of the CNTs in the rolling direction when the concentration is high.

At high magnification (Figure 4-9), in the image of Al-0.1wt% CNT composite reveals the embedded CNTs in the aluminum matrix are observed, also some cracks and breakage of the CNTs is visible which resulted from the compressive force on the CNTs, as explained in chapter 3.

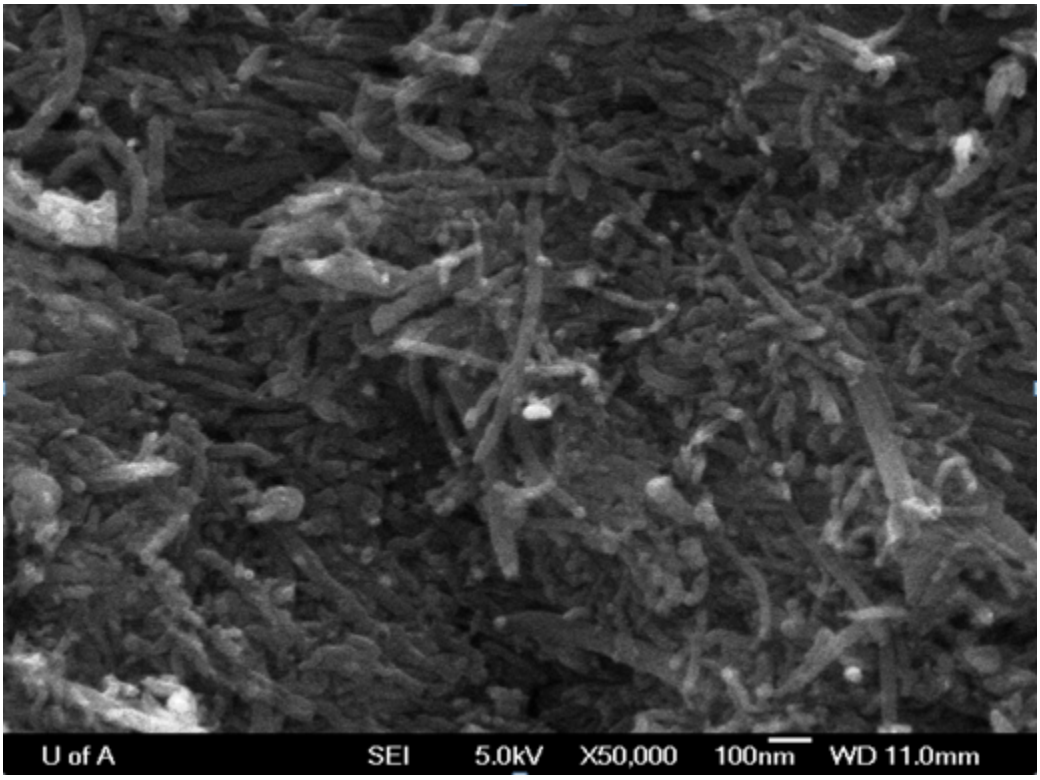

Figure 4-7: SEM image of the interface of the roll bonded 0.23wt%CNT composite sheets after being mechanically delaminated.

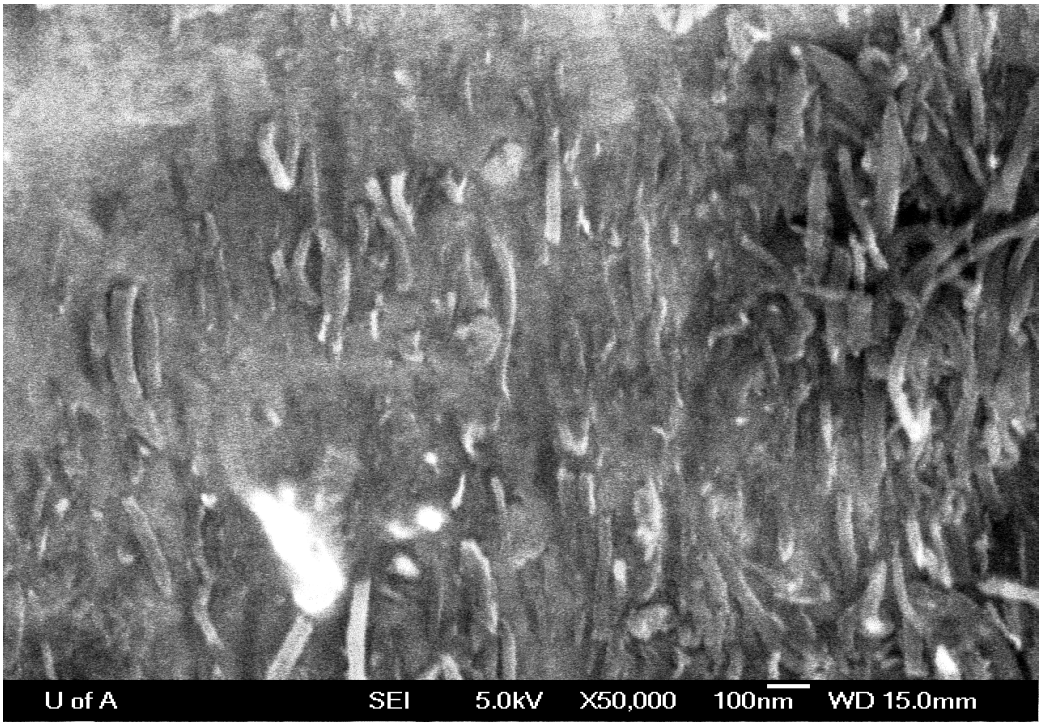

Figure 4-8: SEM image of the interface of the roll bonded 0.1wt%CNT composite sheets after being mechanically delaminated.

Figure 4-9: SEM image of the interface of the roll bonded 0.1wt%CNT composite sheets after being mechanically delaminated, showing the broken CNTs and the deformation of Al where the CNTs were pulled out due to delamination of the composite.

4.3.2 Mechanical properties

Elastic behavior

Mechanical properties of the roll bonded composite were evaluated in terms of elastic modulus in order to gain a better understanding on the elastic deformation characteristics and the influence of the CNTs on other mechanical properties.

The bending stiffness of the roll bonded Al-CNT composites was measured using cantilever bending test. The measurments was performed 5 times for each sample, and the avarage value is reported in Figure 4-10. It is clear that the ARB processed aluminum foil with the lowest CNT content has the highest bending stiffness values measured. Increasing the CNT content decreases the stiffness; however, a sudden increase in stiffness is observed at Al-0.238 wt%CNT. These stiffness observations, when correlated with SEM investigation, show that dispersion of the CNTs on the aluminum matrix plays a significant role on improving the bond strength at the interface.

The elastic modulus of the same samples, measured by the impulse excitation of vibration method, reported as the average of 5 measurements, are plotted in Figure 4-11.

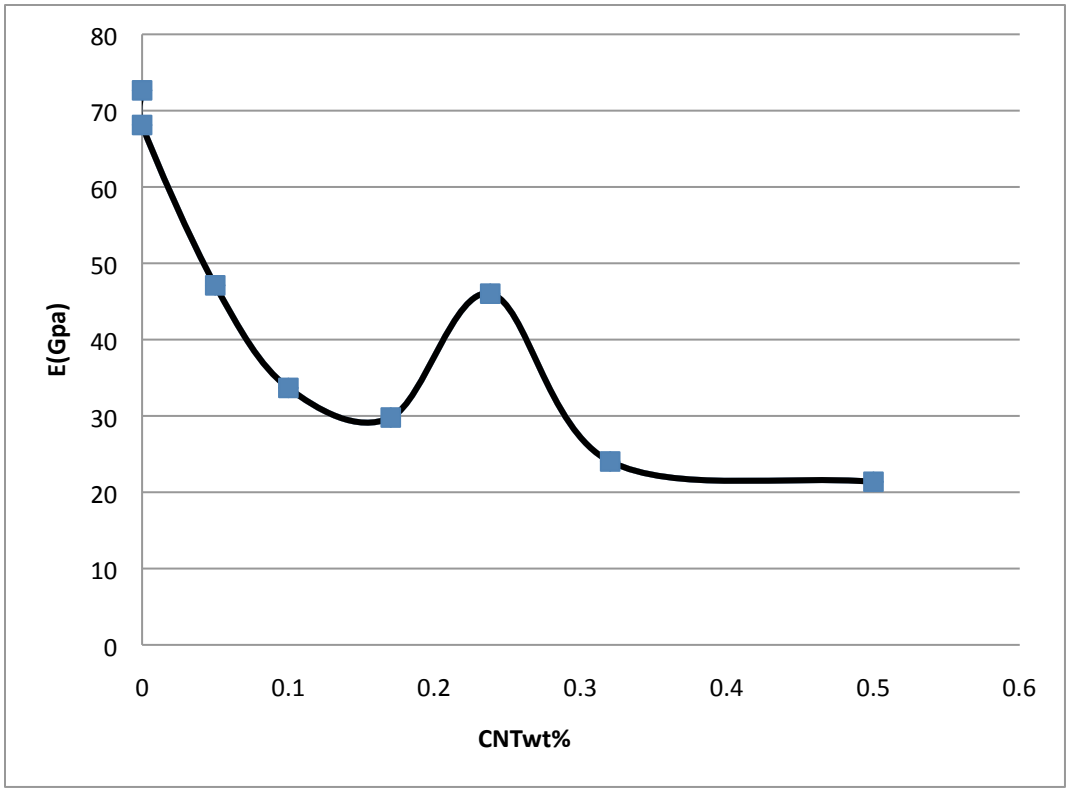

Figure 4-10: elastic modulus value of the composite foils as a function of CNT content measured by cantilever bending test.

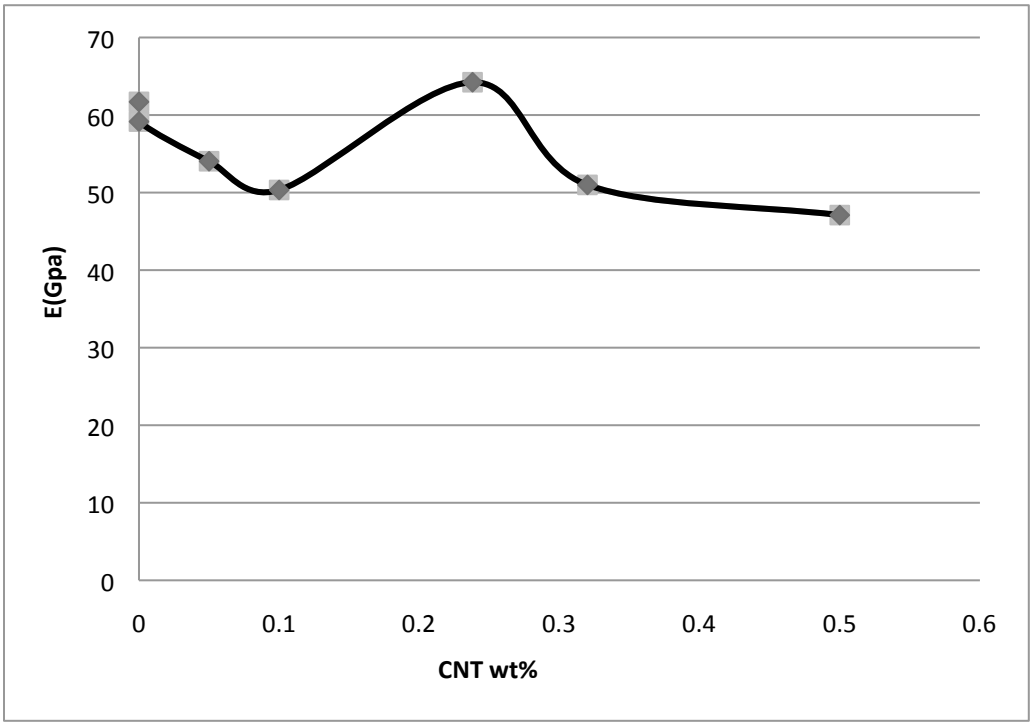

Figure 4-11: Elastic modulus value of the composite foils as a function of CNT content measured by impulse excitation of vibration.

The overall trend of the elastic modulus variation with CNT content of the composite measured by vibration testing corresponds well with the results measured by the cantilever beam test. The concentration of was verified for the 0.23wt% peak result by chemical analysis in order to rule out variation in CNT concentration in different regions of the sheet. The values that were measured by the cantilever beam test are smaller, due to the limitations of this method including the shear effect, the indentation of the load pin on the beam and the movement of the beam in the clamp (clamping method).

Internal friction test

4 aluminum-CNT composite samples were fabricated, with 3 cycles of ARB, at different CNT concentrations as preliminary test conditions. The internal friction results measured by impulse excitation of vibration method and the amount of CNT in each sample by weight percent is given in Table 4-2 below.

Table 4-2: CNT wt% vs. E (GPa) value and their standard deviation measured by Impulse Excitation of Vibration.

Sample name	Internal Friction	Standard deviation
Pure Al annealed	2.852×10^{-3}	5.90×10^{-5}
Pure Al ARB processed	3.417×10^{-3}	1.45×10^{-4}
0.2 wt% CNT	3.045×10^{-3}	1.97×10^{-4}
0.4 wt% CNT	1.3228×10^{-3}	7.41×10^{-3}

Table 4-2 shows the internal friction of the ARB processed commercially pure aluminum sheets and 0.2wt% CNT composites after 3 cycles of ARB. Measurements are reported as the average of 5 measurements using impulse excitation of vibration method. As the table shows, the internal friction of the ARB processed aluminum. The internal friction of the ARB processed samples was 1.2 times higher than the internal friction of a homogenous piece of annealed aluminum base material, which therefore indicates that the ARB process will increase the damping of the aluminum. Moreover, by adding 0.2 and 0.4 wt%

CNT, the internal friction value increased to 3.0×10^{-3} and 1.3×10^{-2}, respectively. In the case of 0.4wt% CNT, the internal friction has shown an increase of about 4.6 times in comparison to bulk aluminum, and 3.9 times as compared to ARB processed aluminum.

To get a better understanding of the effect of different concentration of CNT, on the internal friction of aluminum-CNT, 6 samples with different concentrations of CNTs were made using 5 cycles of ARB. Since the concentrations of CNT in some of the samples were higher than the primary tests, the number of cycles had to be increased in order to achieve satisfactory bonding at the interface. After 5 cycles the samples produced were uniform in shape with no blisters or cracks formed at the edge of the strips.

The results of internal friction after 5 cycles at different CNT concentrations are shown in Figure 4-12. The overall trend is similar to trend that was observed for elastic modulus properties of the composites.

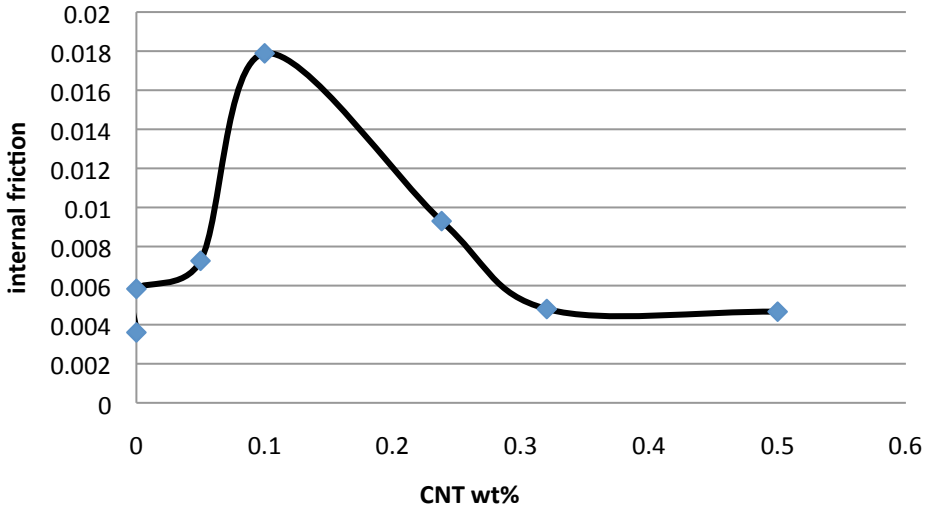

Figure 4-12: Internal friction value of the composite foils as a function of CNT content measured by Impulse Excitation of Vibration.

4.4 Discussion

4.4.1 Role of CNT in elastic strengthening

For a single phase material, the elastic modulus depends on the structure of the material, and therefore, this property may be enhanced if there is a uniform

structure change. For a composite, if there are phases are uniformly distributed in the matrix material, the rule of mixtures can provide an approximation of the elastic modulus of the material. The rule of mixtures states that:

$$E_c = K_c E_f V_f + E_m V_m \qquad \text{(Equation 4-7)}$$

where E_c, E_f and E_m, respectively, are elastic modulus of the composite, CNTs, and the matrix r, and V_f and V_m are the volume fraction of the CNTs in the matrix. K_c, reflects a reinforcement factor; for example, if the fibers are randomly oriented within the matrix, the value of K_c is small. When the calculated E value and the experimental value are matched K_c=1. The dispersion of CNTs in the Al matrix therefore plays an important role in this process [27].

As already mentioned, the deflection of the beam by force (F), is calculated by Equations 4-2 and 4-3.

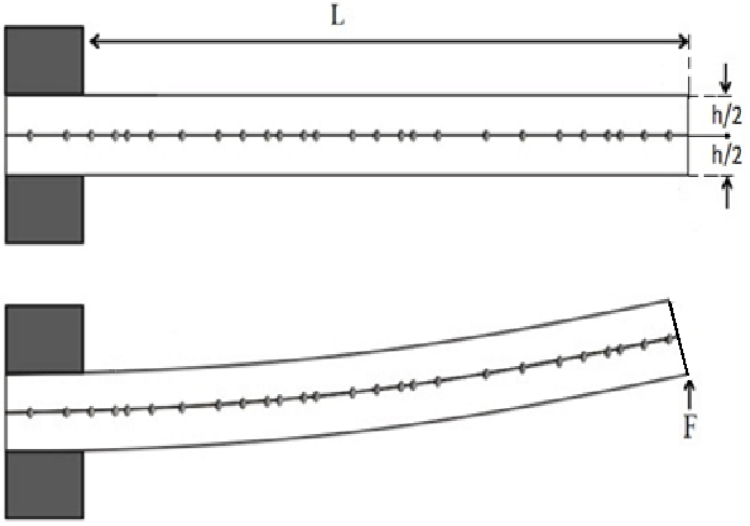

Figure 4-13: Schematic figure of the cantilever beam test setup.

However, these cantilever bending equations assume a monolithic component is in bending. If the layers are not fully bonded, each layer bends separately by a much smaller force, and there will be some force of adhesion between the layers acting only where bonding was successful. The moment of inertia for such sample is much smaller than the sample with the total thickness of

h. Therefore, deflection is higher and a much lower elastic modulus will be observed.

$$I_d = 2I_1 = 2\times[\frac{b(h/2)^3}{12}] = \frac{1}{4}I_b \qquad \text{(Equation 4-8)}$$

Increasing the number of layers by roll bonding therefore leads to lower stiffness. Assuming that a sample with only 2 layers only has half of the interface area is bonded, the total deflection equals the deflection of the bonded part plus the unbounded part, which is more than a bulk sample of the same total thickness. Consequently, with the increase of the CNT content at the initial interface, the strength of the bond decreases, and the observed elastic modulus during bending of the composite decreases.

The sudden increase at 0.23wt% CNT may be explained by the rule of mixtures (Equation 4-7). We are suggesting that at this concentration, CNTs are separated from each other and uniformly distributed in the aluminum matrix. They help the load transfer during the transformation; the load is uniformly distributed between CNTs and the matrix, which results in a higher stiffness observed.

4.4.2 Role of CNT in internal friction of composites

High damping capacity of ultra-fine grained aluminum produced by ARB

It has been observed that high strength [28] and high damping capacity exhibited in ARB processed aluminum, and by adding the total of 0.4wt% CNTs as a reinforcing layer resulted in a large increase in the damping capacity of the composite.

The principle of transmission of vibration is that the vibration transmits through one surface to another. If both of the layers of the sample are rigidly connected and they vibrate as a unit, the transmission loss depends only on the intrinsic damping of the structure of the sample. However, if the sample consists of two or more unconnected layers, the transmission loss depends on the size of the cavity, its absorption, and the properties of the layer. As a result, the transmission loss in such samples is higher than in single layer samples [29]. In

the case of aluminum ARB processed samples, the layered sample acts a multi-layered strip and the transmission loss increases due to the contribution of internal friction at the interfaces between the layers.

The mechanism of high damping capacity needs to be considered in more detail, since the contribution of the ARB process and the addition of CNTs to the microstructure may both have a role. In the case of ARB processed pure aluminum, it has been shown that this microstructure consists of fine grains separated by high angle boundaries [30], and these boundaries display viscous-like properties which convert mechanical energy into thermal energy as a result of internal friction at grain boundaries. This thermal energy will then be dissipated by the conductivity of the metal and heat exchange with surroundings. The amount of energy absorbed at the grain boundary is dependent on the magnitude of shear stress and the grain boundary per unit volume [24,26], Also, at the interfaces between the layers of ARB processed aluminum, the crystal structure of the metal matrix is distorted due to the effect of factors such as plastic deformation caused by wire brushing (i.e. increase in dislocation density near the interface), grain refinement at the interface, and oxide particles that are imbedded at the interface during ARB processing. These factors will affect the damping behavior of the layered composite. A significant number of dislocations are observed in ultrafine grain aluminum sheets which are a possible source of high internal friction because of the motion of the dislocations under loading [26], as was mentioned in section 4-2-6. The high damping of aluminum ARB processed sheets was directly related to the damping mechanisms that were mentioned earlier, and the overall damping is a result of these contributions from dislocation damping, grain boundary damping and interface damping. On the other hand, when comparing the internal friction values of 0.2wt% and 0.4wt% CNT composites, the internal friction value of the 0.4wt% CNT composite has increased significantly. At a concentration of 0.2 wt%, the amount of nanotubes at the interface may be below the minimum threshold value to increase the mechanical properties of the composite, and therefore the observed mechanical properties of the composite is lower than the base material This may be due to the

critical concentration not being achieved in the composite to yield an improvement in properties [31], since sufficient numbers of CNTs may not be present at the interface to increase the internal friction. In this case, the mechanical vibration travels through the aluminum base material, and since the bond strength at the interface is lower than the pure ARB processed aluminum, this composite exhibit lower damping capacity than pure aluminum.

According to the preliminary test results, at concentration of 0.4wt% CNT, internal friction increases significantly, in comparison to pure ARB processed aluminum, this concentration appears to be above the threshold point which leads to an increase in mechanical properties, due to the presence of more CNT/Al interfaces. As discussed, these have a positive contribution on damping capacity of the composites and the transmission loss increases significantly.

Comparing the results for the samples that were made by 5 ARB cycles, the internal friction in the composite increases with increasing CNT amount in the composite; the maximum internal friction was observed at 0.1wt%, but after this point, internal friction of the composite decreases significantly. It has been shown that the efficiency of load transfer from the matrix to the nanotubes is dependent on the quality of the adhesion between the matrix and the nanotubes [32-34].

There are two mechanisms that are responsible for observed mechanical damping. The energy dissipation cause by interfacial sliding at the interface of the nanotubes and the matrix, and the energy dissipation that is caused by the sliding of nanotube-nanotube interfaces.The fine scale and high aspect ratio of the nanotubes results in large interfacial area, which promotes high energy dissipation during sliding of nanotube surfaces within the composite during vibrations [33].
SEM characterization revealed a network of densely packed carbon nanotube clusters at higher surface densities (higher 0.1wt% CNT), the nanotubes are tangled in these bundles, which inhibits the interfacial slip between the tubes, which reduces the efficiency of energy dissipation [33]. Poor load transfer between the nanotube (in bundles), and the surrounding matrix results in less interfacial slipping, and reduced performance. It is possible that some optimum concentration achieves enhanced damping and stiffness properties, however only

one sample exhibited improved properties compared the base material. As a result, further testing is required at other concentrations to confirm this observation. It appears that at higher concentrations, there are more CNT cluster and bundles are formed leading to poor load transfer from the matrix to the CNTs which reduces the damping performance of the composite.

4.5 Conclusion

The elastic modulus and damping capacity of the composites were investigated by cantilever bending test and impulse excitation method. The distribusion of the CNT material at the interface of the metal sheets plays a significant role on these properties. These experiments revealed that up to 0.23wt% of carbon nanotube, the elastic modulus increased, according to the rule of mixtures. Increasing CNTs after 0.23 wt% leads to decrease in elastic behavior of the composite strips. This was due to agglomeration of CNTs at higher concentrations, and that the roll bonding method is not effective on dispersion and aligning the CNTs in the rolling direction when they become entangled. Up to 0.1wt%CNT, the damping behavior of the Al-CNT composites increases in comparison to annealed bulk aluminum, due to the contributions of dislocation damping, grain boundary damping and interface damping in addition to effect of CNTs at the interface. Exceeding from this concentration reduces the energy dissipation due to formation of bundles at higher surface density.

4-6 Bibliography

[1] N. Tsuji, Y. Saito, S.H. Lee, Y. Minamino, Advanced Engineering Materials 5 (2003) 338-344.

[2] V. Segal, Materials Science and Engineering A 197 (1995) 157-164.

[3] R.Z. Valiev, Materials Science 234-236 (1997) 59-66.

[4] X. Huang, N. Kamikawa, N. Hansen, Materials Science and Engineering: A 483-484 (2008) 102-104.

[5] D. Hughes, N. Hansen, Acta Materialia 48 (2000) 2985-3004.

[6] O. Sitdikov, T. Sakai, a Goloborodko, H. Miura, R. Kaibyshev, Philosophical Magazine 85 (2005) 1159-1175.

[7] H. Zhang, Z. Hei, G. Liu, K. Lu, Acta Materialia 51 (2003) 1871-1881.

[8] G. Krallics, J.G.Lenard, Journal of Materials Processing Technology 152 (2004) 154-161.

[9] N. Tsuji, Y. Ito, Y. Saito, Y.Minamino, Scripta Materialia 47 (2002) 893-899.

[10] Y. Saito, N. Tsuji, H. Utsunomiya, T. Sakai, R.G. Hong, Acta Metallurgica 39 (1998) 1221-1227.

[11] M. Eizadjou, H.D. Manesh, K. Janghorban, Journal of Alloys and Compounds 474 (2009) 406-415.

[12] Q. Liu, X. Huange D. Lloyd, N. Hansen, Acta Materialia 50 (2002) 3789-3802.

[13] N. Kamikawa, X. Huang, N. Tsuji, N. Hansen, Acta Materialia 57 (2009) 4198-4208.

[14] S.H. Lee, Y. Saito, N. Tsuji, H. Utsunomiya, T. Sakai, Scripta Mater. 46 (2002) 281–285.

[15] M. Shaarbaf, M. Toroghinejad, Materials Science and Engineering: A 473 (2008) 28-33.

[16] N. Hansen, X. Huang, R. Ueji, N. Tsuji, Materials Science and Engineering A 387-389 (2004) 191-194.

[17] G. Fougere, L. Riester, M. Ferber, J. Weertman, R. Siegel, Materials Science and Engineering A 204 (1995) 1-6.

[18] G.P. Sanders, J.A. Eastman, J.R. Weertman, Acta Metallurgica 45 (1997) 4019-4025.

[19] D. Chen, Materials Science and Engineering A 190 (1995) 193-198.

[20] V. Krstic, U. Erb, G. Palumbo, Scripta Metallurgica et Materialia 29 (1993) 1501-1504.

[21] H.S. Kim, M.B. Bush, Acta Metallurgica 11 (1999) 361-367.

[22] "Standard Test Method For Dynamic Young's Modulus, Shear Modulus, and Poisson's Ratio By Impulse Excitation of Vibration", ASTM designation: E1876-09, Pennsylvania: American society for Testing Materials-ASTM, 2009.

[23] M.S. Blanter, I.S. Golovin, H. Neuhauser, H.R. Sinning, Internal Friction In Metallic Materials, Springer Verlag, 2007.

[24] E.J. Lavernia, R.J. Perez, J. Zhang, Metallurgical and Materials Transactions A 26 (1995) 2803-2818.

[25] H. Lu, X. Wang, T. Zhang, Z. Cheng, Q. Fang, Materials 2 (2009) 958-977.

[26] Y. Koizumi, M. Ueyama, N. Tsuji, Y. Minamino, K. Ota, Journal of Alloys and Compounds 355 (2003) 47-51.

[27] H. Choi, J. Shin, B. Min, J. Park, Materials Science 24 (2009) 2610-2616.

[28] R.Z. Valiev, R.K. Islamgaliev, I.V. Alexandrov, Methods 45 (2000) 103-189.

[29] K. Lawrence, F. Austin, C. Alan, S. James, Fundumentals of Acoustics, Third Edition, Wiley, Calefornia, 1982.

[30] X. Huang, N. Tsuji, N. Hansen, Y. Minamino, Materials Science and Engineering A 340 (2003) 265-271.

[31] T.H. Courtney, Mechanical Behavior of Materials, Second Edition, MCGraw-Hill, 2000.

[32] M. Kireitseu, D. Hui, G. Tomlinson, Composites Part B: Engineering 39 (2008) 128-138.

[33] J. Suhr, N. Koratkar, P. Keblinski, P. Ajayan, Nature Materials 4 (2005) 134-137.

[34] J.S. Jang, J. Varischetti, G.W. Lee, J. Suhr, Composites Part A: Applied Science and Manufacturing 42 (2011) 98-103.

5 Conclusions

Accumulative roll bonding may be used to fabricate carbon nanotube reinforced aluminum matrix composites. Transmission electron microscopies confirmed that the nanotubes were embedded into the metal matrix and maintain their multiwalled structure. The number of the cycles and dispersion of the CNTs at the interface of the composites has a significant effect in promoting the bond strength at the interface of the composites. Only nanotubes with diameters >30 nm and more than 30 walls are retained during four consecutive rolling operations at 50% reduction.

It has been suggested that CNTs with smaller diameters and fewer walls may prematurely buckle, and are not likely to survive the rolling process. In these cases, an axial tensile stress during rolling contributes to buckling, and this is lower in CNTs with a larger diameter since these have a higher number of walls with a greater effective cross-sectional area. The buckling process is a precursor to rupture of the CNTs since the formation of kinks and defects occurs during rolling; which leads to rupture of the CNTs since the formation of kinks and defects promote failure.

The elastic deflection and vibration damping capacity of the composites were investigated by cantilever bending test and by the impulse excitation method. The concentration of CNT material at the interface has a strong influence on these properties, and measurements by both methods revealed that up to 0.23wt% of nanotubes increased the elastic modulus according to the rule of mixtures. When the concentration exceeds 0.23wt%, the elastic modulus of the composites shows a sudden decrease, since the load transfer between CNTs and the matrix is no longer effective. This was due to the fact that CNTs tend to agglomerate at high concentrations, and the roll bonding method is not effective dispersing and aligning the CNTs in the rolling direction when they become entangled.

The damping behavior of the composites increases with the addition of up to 0.1wt% nanotube material. The overall damping of the ARB processed aluminum increases in comparison to annealed bulk aluminum. This may be

explained by the contributions from dislocation damping, grain boundary damping and interface damping. With addition of CNT material to the aluminum matrix, the interfacial sliding at the interface of the nanotubes and the matrix, as well as nanotube-nanotube interfaces increases the energy dissipation during vibration. Beyond a critical certain concentration (in this case 0.1wt%), increasing the amount of CNT material is detrimental since they form bundles with reduced energy dissipation efficiency.

Future work

The mechanical properties of Al-CNT laminated composites have not been investigated by many researchers. Since the CNTs have much higher stiffness than the metal substrate, they have the potential for a variety of applications such as acoustic and structural applications.

It was shown in this study that the major issue of fabrication of Al-CNT laminated composites is agglomeration of the CNTs at the interface, which leads to weakening the interfacial bond and degradation of the mechanical performance of these composites.

The bond strength and mechanical properties of aluminum ARB processed aluminum has also shown improvement when SiO_2 nanoparticles are added at the interface of the rolled aluminum sheets. Therefore, as the next step to improve mechanical performance Al-CNT laminated composite, it is important to investigate the mechanical performance such as fracture toughness and stress and elastic modulus of these composites when SiO_2 nanoparticles are added in a mixture with CNTs at the interface.